Scientific Report No. 2
Contract N140(70024)75686B
December 1964

• p m l • a p p l i e d • m a t h e m a t i c s • •

Toroidal Wave Functions and Their Application to the Free-Flooding Ring Transducer

by

Charles H. Sherman
N. G. Parke

for

U. S. Navy Underwater Sound Laboratory

PARKE MATHEMATICAL LABORATORIES, Inc.
One River Road • Carlisle, Massachusetts

• p m l • a p p l i e d • m a t h e m a t i c s • •

PARKE MATHEMATICAL LABORATORIES, INCORPORATED
ONE RIVER ROAD • CARLISLE, MASSACHUSETTS

Requests for additional copies by Agencies of the Department of Defense, their contractors, and other Government agencies should be directed to the:

DEFENSE DOCUMENTATION CENTER (DDC)
CAMERON STATION
ALEXANDRIA, VIRGINIA

Department of Defense contractors must be established for DDC services or have their 'need-to-know' certified by the cognizant military agency of their project or contract.

All other persons and organizations should apply to the:

U.S. DEPARTMENT OF COMMERCE
OFFICE OF TECHNICAL SERVICES
WASHINGTON 25, D.C.

A limited number of copies are also available by writing to:

PARKE MATHEMATICAL LABORATORIES, INC.
ONE RIVER ROAD
CARLISLE, MASSACHUSETTS

BLANK PAGE

Scientific Report No. 2
Contract N140(70024)75686B
December 1964

• p m l • a p p l i e d • m a t h e m a t i c s • •

Toroidal Wave Functions and Their Application
to the Free-Flooding Ring Transducer

by

Charles H. Sherman
N. G. Parke

for

U. S. Navy Underwater Sound Laboratory

PARKE MATHEMATICAL LABORATORIES, Inc.
One River Road • Carlisle, Massachusetts

• p m l • a p p l i e d • m a t h e m a t i c s •

PARES MATHEMATICAL LABORATORIES, INCORPORATED
ONE RIVER ROAD • CARLISLE, MASSACHUSETTS

Abstract

V. H. Weston has derived solutions of the wave equation in toroidal coordinates which can be used to solve the problem of acoustic radiation from a torus. The wave equation is not separable in toroidal coordinates and special methods are required to obtain solutions. Weston's solutions are not orthogonal functions, which also requires special methods in applying them to radiation problems. However, the special case of a torus of infinitesimally thin cross section can be solved by the usual methods, and in this report this thin torus problem is worked out in detail. The usefulness of this problem as a theoretical model for free-flooding ring transducers is shown by comparison of calculations and measurements. The calculation of toroidal wave functions is also discussed, and numerical results are given for those functions which are needed in transducer problems.

PARRE MATHEMATICAL LABORATORIES, INCORPORATED
ONE RIVER ROAD • CARLISLE, MASSACHUSETTS

Table of Contents

PARKE MATHEMATICAL LABORATORIES, INCORPORATED
ONE RIVER ROAD • CARLISLE, MASSACHUSETTS

Toroidal Wave Functions and Their Application to the Free-Flooding Ring Transducer

by

Charles H. Sherman and N. G. Parke

Introduction

Development work with free-flooding ring transducers for acoustic applications has long suffered from the lack of a theoretical description of the sound field of this type of vibrator. Typical shape and an approximate velocity distribution for such ring transducers are shown in Fig. 1a. The torus with an appropriately chosen velocity distribution, as shown in Fig. 1b, could be expected to be a useful model for obtaining a theoretical treatment which would be approximately applicable to ring transducers. The torus has the correct topology, which is the essential requirement for a model. However, its circular cross section is a serious departure from actual transducer shapes which might be an important factor.

The toroidal coordinate system[1] is appropriate for this problem because one of the families of constant coordinate surfaces is a set of tori. The first basic difficulty that one encounters in the problem of acoustic radiation from a torus is that the Helmholtz equation is not separable in toroidal coordinates. Fortunately, Weston[2] has developed a method of solving the Helmholtz equation in non-separable, rotational coordinate systems and has derived in particular detail a set of wave functions

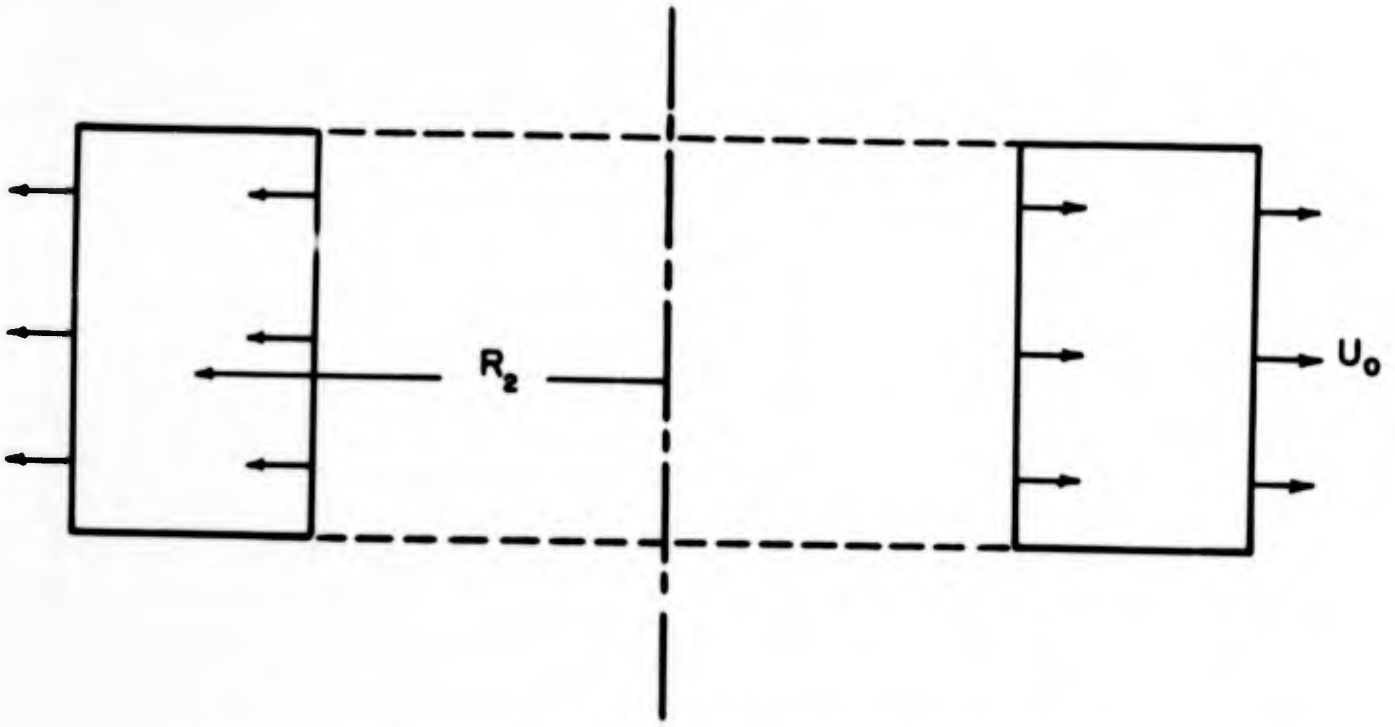

Fig. 1a. Ring Transducer — the arrows indicate an approximation to the motion of the surfaces.

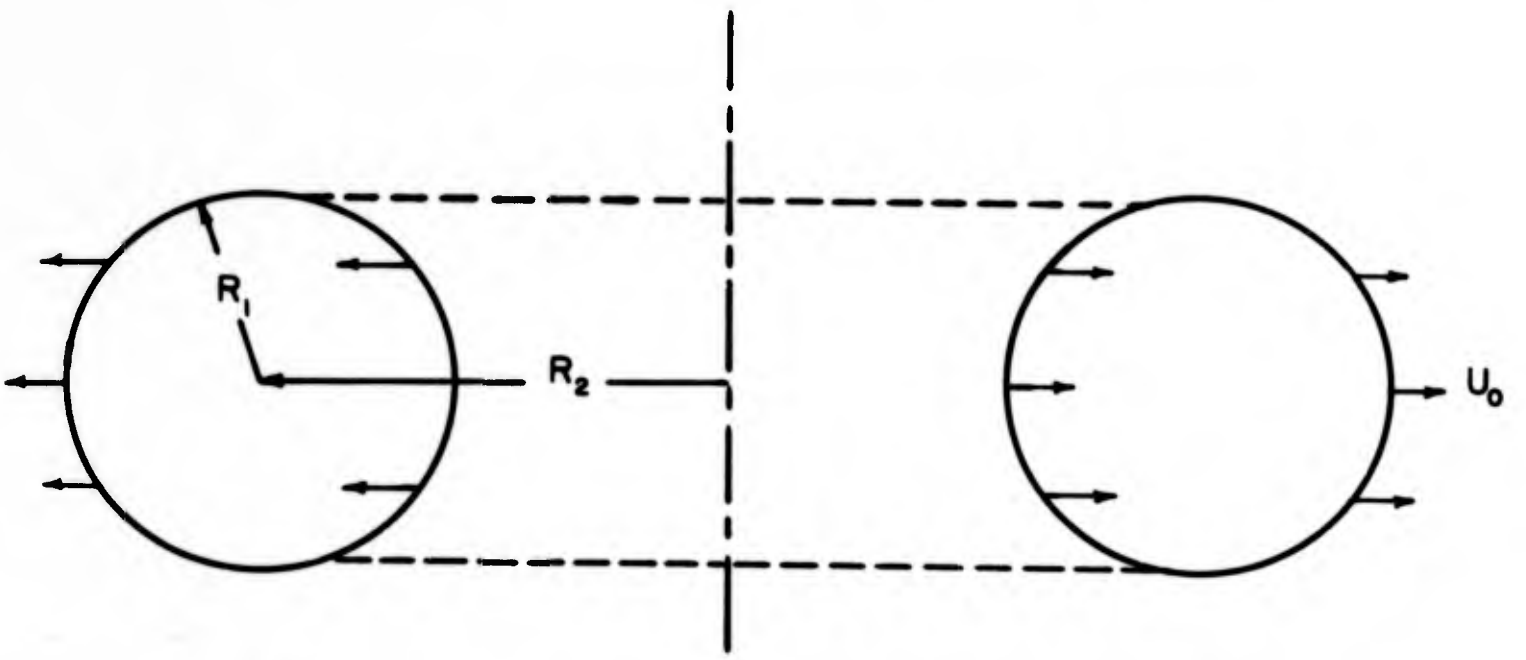

Fig. 1b. Torus with a velocity distribution which approximates the motion of a ring transducer.

for toroidal coordinates.[3] He applied a special case of these wave functions to the problem of scattering of electromagnetic waves from a thin ring,[4] but there appears to have been no other application to physical problems.

It is our object in the present work to apply Weston's toroidal wave functions to the general problem of acoustic radiation from tori with special attention being given to obtaining theoretical results that will be useful in the development of ring transducers. This report will describe those parts of the program which are reasonably complete. Methods for calculating Weston's wave functions will be described, and a table of numerical results will be given. The acoustic calculations will here be confined to the special case of thin tori ($R_2/R_1 >> 1$, see Fig. 1b). In this case it is possible to satisfy the boundary conditions by use of asymptotic approximations to the wave functions which are orthogonal, and results can be obtained with little numerical work. Various calculations will be compared with measurements on single ring transducers and co-axial arrays of ring transducers, and we will find that the thin torus solution has considerable practical usefulness. It also provides a relatively simple situation in which to investigate questions such as the effects of different velocity distributions.

We are also carrying out numerical calculations for the general problem of radiation from a torus of arbitrary cross sectional size and from a toroid of rectangular cross sectional shape. These cases, which involve a large amount of numerical work, will be described in later reports.

Some of the work to be described here has been presented in a preliminary fashion in an earlier technical memorandum.[5] The only other theoretical work that we are aware of which may have application to the free-flooding ring transducer problem is that of Junger[6] and Chin.[7]

Weston's Toroidal Wave Functions

The Functions Needed for Transducer Problems

There are many descriptions of the toroidal coordinate system, but no standard notation is in use. Moon and Spencer,[1] for example, give a complete description using the notation η, θ, χ for the toroidal coordinates. We'll follow Weston's notation and use s, η, φ respectively (ξ is also used by Weston where $s = \cosh \xi$). The coordinate φ is the usual azimuthal angle (identical with the φ in spherical coordinates). Surfaces of constant s are tori centered on the origin with $s = \infty$ being a ring in the x-y plane and smaller values of s corresponding to thicker and thicker tori until $s = 1$ is a torus consisting of the z-axis and a surface at infinity. Surfaces of constant η are portions of spheres; η has the range $-\pi \leq \eta \leq \pi$ and measures location around the cross section of a torus. The toroidal coordinate system also has a parameter d which is the radius of the ring which the tori reduce to as $s \to \infty$. Figure 2 illustrates some features of the toroidal coordinates; other details will be found in the Appendix.

It should be noted that one frequently sees references to torus functions[8] or toroidal harmonics.[9] These are Legendre functions of half

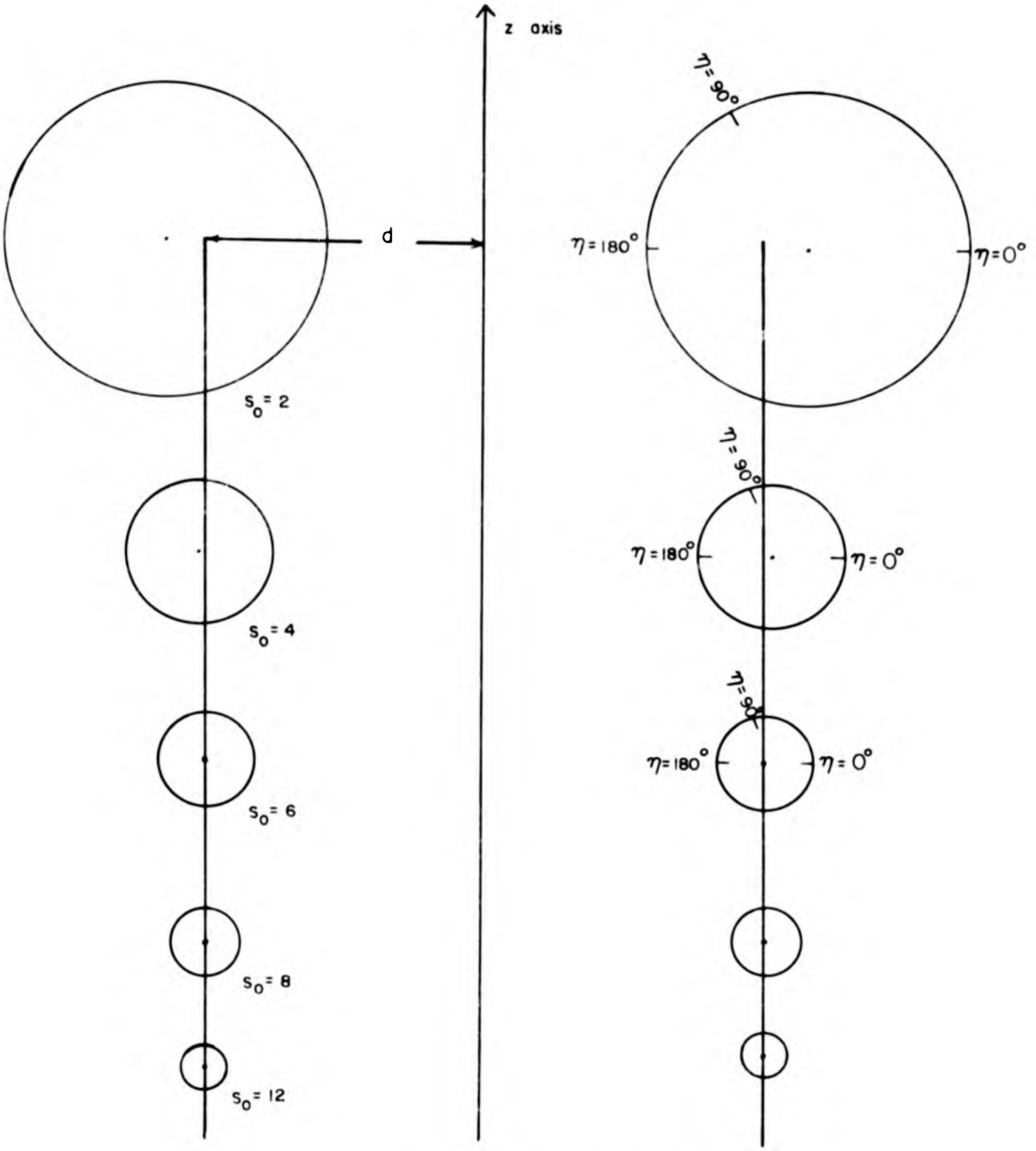

Fig. 2 Illustration of the relative dimensions of tori for fixed d and different values of s_0

integer order and are solutions of Laplace's equation in toroidal coordinates. Laplace's equation is R-separable[1] in toroidal coordinates and solutions can be obtained easily compared to the Helmholtz equation.

Weston[3] has shown that any solution of the Helmholtz equation which is continuous and single valued outside the torus $s = s_0$ (i.e., the region $1 \le s \le s_0$) and satisfies the radiation condition and arbitrary boundary conditions on the torus can be represented by a linear combination of the toroidal wave functions (reference 3, p. 255; page references to Weston will frequently be given)

$$e^{im\varphi} V^{M}_{M+2\ell}(s,\eta),$$

and

$$e^{im\varphi} W^{M}_{M+2\ell+1}(s,\eta),$$

where

$$m = 0, \pm 1, \pm 2, \ldots$$
$$M = |m|$$
$$\ell = 0, 1, 2, \ldots$$

The V and W functions have the following structure as a result of satisfying the radiation condition (3, p. 248):

$$V^{M}_{M+2\ell}(s,\eta) = S^{M}_{M+2\ell}(s,\eta) + i(-1)^{M+2\ell+1} S^{M}_{-M-2\ell-1}(s,\eta), \tag{1}$$

$$W^{M}_{M+2\ell+1}(s,\eta) = T^{M}_{M+2\ell+1}(s,\eta) + i(-1)^{M+2\ell+2} T^{M}_{-M-2\ell-2}(s,\eta), \tag{2}$$

where (3, p. 249)

$$S^{M}_{N} = \tag{3}$$

$$\frac{\Gamma(N+M+1)\pi^{1/2}(-1)^{M}(kd)^{N}}{\Gamma(N-M+1)\,2^{\frac{M+N}{2}+1}(s-\cos\eta)^{\frac{M+N}{2}}} \sum_{p=0}^{\infty} \frac{(kd)^{2p}(-1)^{p}}{(s-\cos\eta)^{p}\,2^{p}} \frac{1}{p!\,\Gamma(N+3/2+p)} \sum_{r=0}^{\ell} \frac{\left(\frac{M-N}{2}\right)_r \left(\frac{N+M+1}{2}\right)_r}{r!\,(s-\cos\eta)^{r}} (s^2-1)^{r/2} P^{-M-r}_{p+\frac{N+M}{2}}(s)$$

$$T^{M}_{N} = \tag{4}$$

$$\frac{\Gamma(N+M+1)\pi^{1/2}(-1)^{M}\sin\eta\,(kd)^{N}}{\Gamma(N-M+1)\,2^{\frac{M+N+3}{2}}(s-\cos\eta)^{\frac{M+N+1}{2}}} \sum_{p=0}^{\infty} \frac{(kd)^{2p}(-1)^{p}}{(s-\cos\eta)^{p}\,2^{p}} \frac{1}{p!\,\Gamma(N+3/2+p)} \sum_{r=0}^{\ell} \frac{\left(\frac{M-N+1}{2}\right)_r \left(\frac{M+N}{2}+1\right)_r}{r!\,(s-\cos\eta)^{r}} (s^2-1)^{r/2} P^{-M-r}_{p+\frac{M+N-1}{2}}(s)$$

In Eqs. (3) and (4) the subscript N can be specialized to either of the values required in Eqs. (1) and (2), and the symbol $(a)_b$ is Pochhammer's notation for $\Gamma(a+b)/\Gamma(a)$.

In the acoustic radiation problems which are being contemplated now there are two types of symmetry which restrict the wave functions we'll need to special cases of those above. In our problems the surface of the torus will be vibrating with axial symmetry and with symmetry with respect to the x-y plane. The first symmetry means that the resulting sound fields do not depend on φ which requires wave functions with $m=0$ and $M=0$. The second symmetry means that the sound fields are even functions of η which requires the V functions only, since the V functions are even functions of η and the W functions are odd functions of η. The set of wave functions which we need then are:

$$V_{2\ell}(s,\eta) = S_{2\ell}(s,\eta) + i(-1)^{2\ell+1} S_{-2\ell-1}(s,\eta), \tag{5}$$

where

$$S_N = \frac{\pi^{1/2}(kd)^N}{2^{N/2+1}(s-\cos\eta)^{N/2}} \sum_{p=0}^{\infty} \frac{(kd)^{2p}(-1)^p}{(s-\cos\eta)^p 2^p} \frac{1}{p!\,\Gamma(N+3/2+p)} \sum_{r=0}^{\ell} \frac{(-\frac{N}{2})_r (\frac{N+1}{2})_r}{r!\,(s-\cos\eta)^r} (s^2-1)^{r/2} P^{-r}_{p+\frac{N}{2}}(s). \tag{6}$$

To illustrate the situation more completely the lowest order wave function $(\ell=0)$ is:

$$V_0(s,\eta) = S_0(s,\eta) - i S_{-1}(s,\eta), \tag{7}$$

where

$$S_0 = \frac{1}{2}\pi^{1/2} \sum_{p=0}^{\infty} \frac{(kd)^{2p}(-1)^p}{(s-\cos\eta)^p 2^p} \frac{1}{p!\,\Gamma(3/2+p)} P_p(s) \tag{8}$$

$$S_{-1} = \frac{\pi^{1/2}(s-\cos\eta)^{1/2}}{2^{1/2}\,kd} \sum_{p=0}^{\infty} \frac{(kd)^{2p}(-1)^p}{(s-\cos\eta)^p 2^p} \frac{1}{p!\,\Gamma(1/2+p)} P_{p-1/2}(s). \tag{9}$$

In addition to the series representation given above Weston derived an integral representation for the toroidal wave functions (3, p. 251). When Weston's result is specialized to the case of interest here it can be shown that

$$V_{2\ell}(s,\eta) = (-1)^{\ell} \frac{2^{2\ell}(\ell!)^2}{\pi(2\ell)!} \int_0^{\pi} P_{2\ell}(z(t))\, h_{2\ell}^{(1)}(x(t))\, dt. \tag{10}$$

$P_{2\ell}$ and $h_{2\ell}^{(1)}$ are respectively the Legendre polynomial and spherical Hankel function of the first kind, where

$$z(t) = \frac{(s^2-1)^{1/2} \sin t}{\sqrt{2}\,(s-\cos\eta)^{1/2}\,[s+(s^2-1)^{1/2}\cos t]^{1/2}}, \tag{11}$$

and

$$X(t) = \sqrt{2}\,kd \left[\frac{s+(s^2-1)^{1/2}\cos t}{s-\cos\eta}\right]^{1/2}. \tag{12}$$

This integral representation of the toroidal wave function has an interesting physical interpretation. It can be shown that $X(t)$ is equal to kR where k is the wave number and R is the distance from a point on the ring $s=\infty$ specified by the integration variable t to the field point (s,η). It can also be shown that $z(t)$ is equal to $\cos\delta$ where δ is the angle between a tangent to the ring at the point specified by t and the line from that point on the ring to the field point. Thus Eq. (10) represents $V_{2\ell}(s,\eta)$ as an integral over a continuous distribution of spherical wave sources of order 2ℓ on a ring.

Either the series representation in Eq. (6) or the integral representation in Eq. (10) can be used to compute numerical values of the wave functions and their derivatives. We have made calculations by both

methods and compare some of them in Table 1. The series converges readily

Table 1

Comparison of Numerical Values of

Toroidal Wave Functions

Function	s	η	Calculated from Integral	Calculated from Series
S_{0}	8	0°	.2121	.2121
S_{0}	8	45°	.2244	.2244
S_{1}	8	0°	.1125	.1183
S_{1}	8	45°	.1161	.1217
S_{2}	8	0°	-.0526	-.0519

as long as s is not too small and ξ_0 is not too large, and under these conditions is more convenient than the integral for calculating the functions themselves. When convergence of the series is poor the integral representation can be evaluated numerically; it has the advantage of involving better tabulated functions than the series. We are using the integral for the calculation of derivatives of the wave functions.

In tables 2, 3, and 4 we give numerical values for the wave functions V_0, V_2 and V_4 as calculated from the series representation. Some of these results are plotted in Fig. 3 which shows the behaviour of the $S_0(s, \eta)$ function.

The Far Field Functions

Weston derived the asymptotic forms for the toroidal wave functions in the far field (3, p. 251). He expressed the toroidal coordinates s

Table 2 The Toroidal Wave Functions S_0 and S_{-1}

	S_0				S_{-1}			
				kd = 1				
η \ s	2	4	6	8	6	8	10	
0°	.4952	.6341	.6650	.6785	.5882	.7092	.7984	
45°	.5824	.6609	.6804	.6893	.6282	.7402	.8241	
90°	.7093	.7120	.7125	.7127	.7208	.8132	.8846	
135°	.7775	.7498	.7387	.7328	.8080	.8828	.9430	
180°	.7981	.7628	.7483	.7404	.8426	.9109	.9666	
				kd = 2				
0°	.04004	.1607	.1958	.2121	.06893	.1183	.1563	
45°	.0808	.1856	.2123	.2244	.07171	.1217	.1599	
90°	.2189	.2468	.2520	.2538	.08295	.1326	.1701	
135°	.3388	.3046	.2903	.2825	.09942	.1464	.1821	
180°	.3802	.3268	.3056	.2941	.10745	.1528	.1875	

Table 3 The Toroidal Wave Functions S_2 and S_{-3}

	S_2			S_{-3}		
kd = 1						
η \ s	6	8	10	6	8	10
0°	.005569	.009780	.01215	-4.0381	-5.8410	-7.6767
45°	.01213	.01409	.01521	-2.4986	-3.7628	-5.0501
90°	.02324	.02209	.02145	+1.5653	+1.5944	+1.6369
135°	.02995	.02759	.02617	+6.0891	+7.4385	+10.1151
180°	.03187	.02933	.02772	+8.0893	+9.9854	+11.8902
kd = 2						
0°	-.06725	-.05193	-.04400	-.7623	-1.0144	-1.2639
45°	-.04501	-.03680	-.03264	-.5495	-.7380	-.9213
90°	-.00256	-.00603	-.008076	+.0069	-.0269	-.0523
135°	+.02785	+.01802	+.01188	+.6183	+.7398	+.8747
180°	+.03780	+.02638	+.01908	+.8861	+1.0727	+1.2746

Table 4 The Toroidal Wave Functions S_4 and S_{-5}

	S_4			S_{-5}		
			kd=1			
η \ s	6	8	10	6	8	10
0°	$.1589 \times 10^{-3}$	$.1737 \times 10^{-3}$	$.1813 \times 10^{-3}$	233.3	476.4	808.0
45°	$.1372 \times 10^{-3}$	$.1715 \times 10^{-3}$	$.1856 \times 10^{-3}$	-86.10	-135.7	-168.0
90°	$.2112 \times 10^{-3}$	$.2227 \times 10^{-3}$	$.2266 \times 10^{-3}$	-361.6	-671.7	-1072
135°	$.3220 \times 10^{-3}$	$.2987 \times 10^{-3}$	$.2845 \times 10^{-3}$	182.3	226.8	269.2
180°	$.3627 \times 10^{-3}$	$.3294 \times 10^{-3}$	$.3090 \times 10^{-3}$	678.6	1062	1535
			kd = 2			
0°	-.002765	-.002141	-.002049	8.240	16.31	27.17
45°	-.003068	-.002219	-.002008	-2.427	-3.407	-4.370
90°	-.001840	-.001453	-.001380	-12.36	-22.21	-34.83
135°	+.0001346	-.0001613	-.0004018	3.692	4.469	5.231
180°	+.0009176	+.0003974	+.00003395	18.90	29.46	44.12

Fig. 3 The Toroidal Wave Function S_0

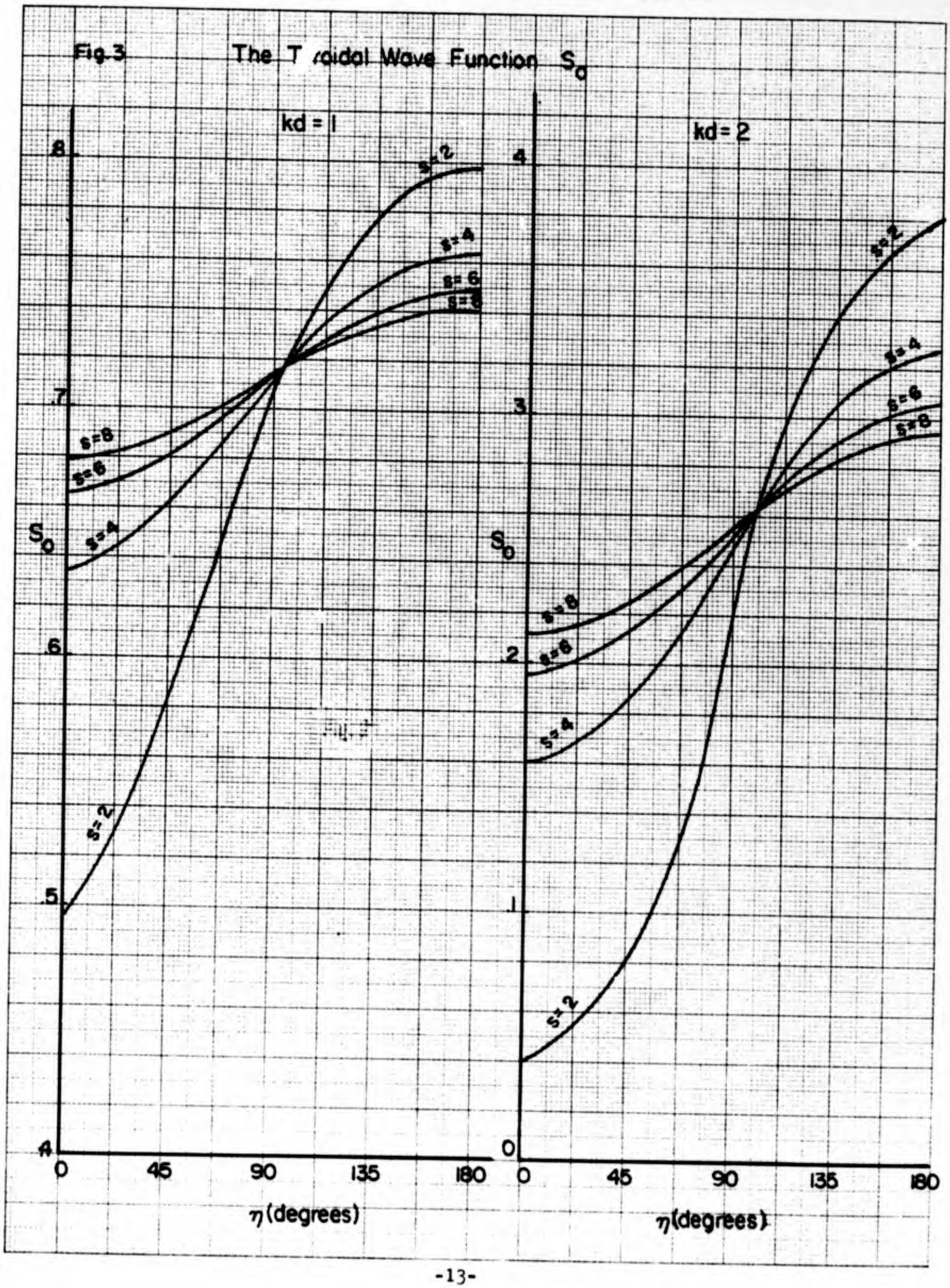

and η in terms of the spherical coordinates r and θ and found the asymptotic form of $V^{M}_{M+2\ell}(r,\theta)$ as $r \to \infty$. His result for the case in which $M = 0$ is

$$V_{2\ell} \to (-i)^{2\ell+1} \frac{e^{ikr}}{kr} R_{2\ell}(\cos\theta), \tag{13}$$

where

$$R_{2\ell}(\cos\theta) = \sum_{p=0}^{\ell} \frac{(-\ell)_p \left(\ell+\frac{1}{2}\right)_p}{p!} \left(\frac{2\sin\theta}{kd}\right)^p J_p(kd\sin\theta). \tag{14}$$

In Figures 4-7 the first four $R_{2\ell}(\cos\theta)$ functions are plotted for $kd = 1$, 2, and 3.

It seems useful to think of the $R_{2\ell}(\cos\theta)$ functions as the basic modes of radiation from a torus in the same sense that the Legendre polynomials give basic modes of radiation from a sphere. This view is supported by the fact that (3, p. 252)

$$R_{2\ell}(\cos\theta) \to P_{2\ell}(\cos\theta), \quad kd \to 0.$$

It should be noted that the lowest order far field function,

$$R_0(\cos\theta) = J_0(kd\sin\theta),$$

is the familiar far field of a circular ring source of zero thickness and radius d.[10]

The Asymptotic Functions for $s \to \infty$.

Weston also derived the asymptotic forms of the wave functions as $s \to \infty$ (3, p. 255). The result of interest here is

$$V_{2\ell}(s,\eta) \to \text{constant} + i \frac{(-1)^{\ell+1} \epsilon_\ell \sqrt{2\pi}}{(kd)^{2\ell+1} \Gamma\left(\frac{1}{2}-2\ell\right)} s^{1/2} P_{\ell-1/2}(s) \cos\ell\eta, \quad s \to \infty, \tag{15}$$

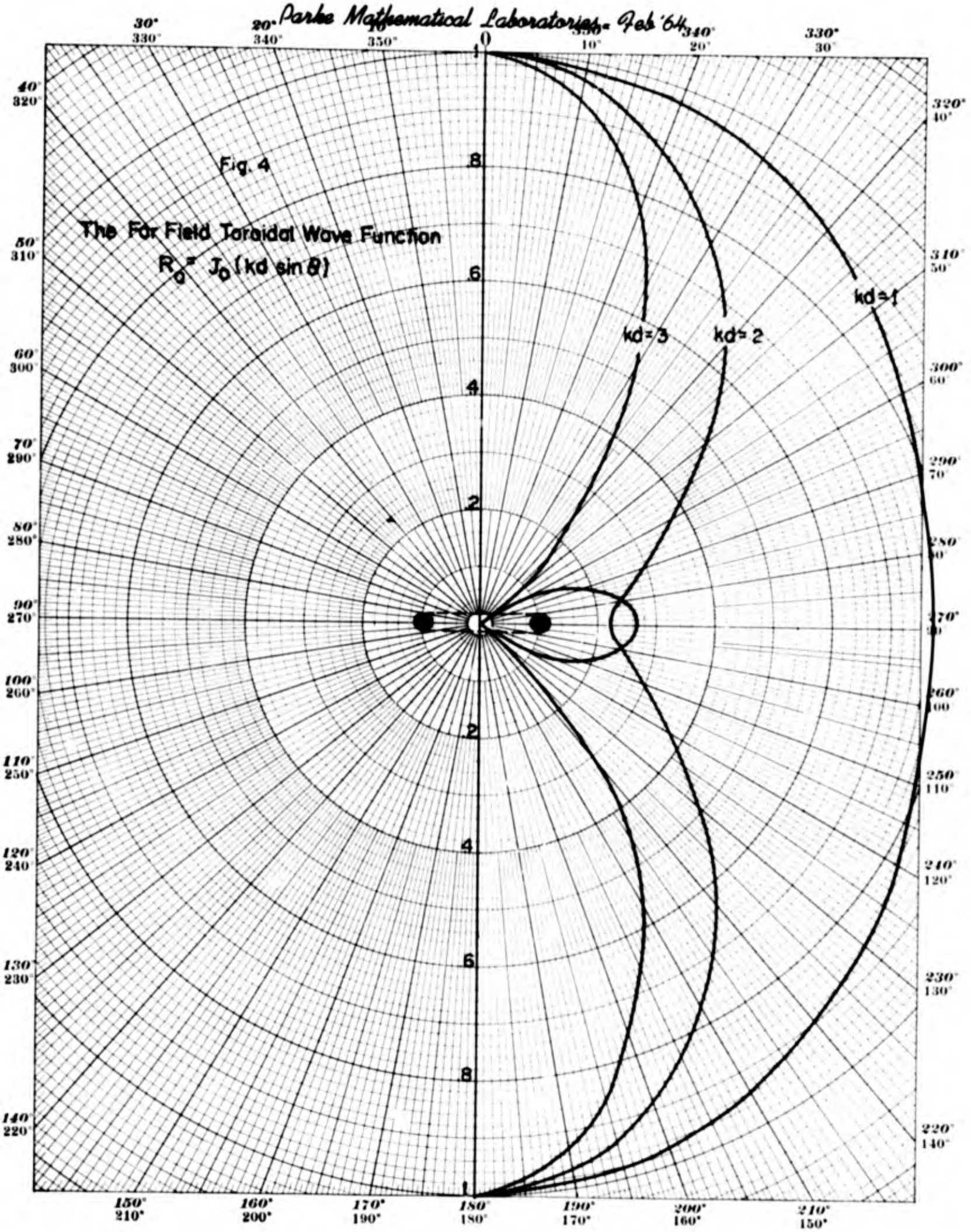
Parke Mathematical Laboratories - Feb '64
Fig. 4
The For Field Toraidal Wave Function
$R_0 = J_0\{kd \sin\theta\}$
kd=3
kd=2
kd=1
0
2
4
6
8
10
20
30
40
50
60
70
80
90
100
110
120
130
140
150
160
170
180
190
200
210
220
230
240
250
260
270
280
290
300
310
320
330
340
350

Parke Mathematical Laboratories - Feb. '64

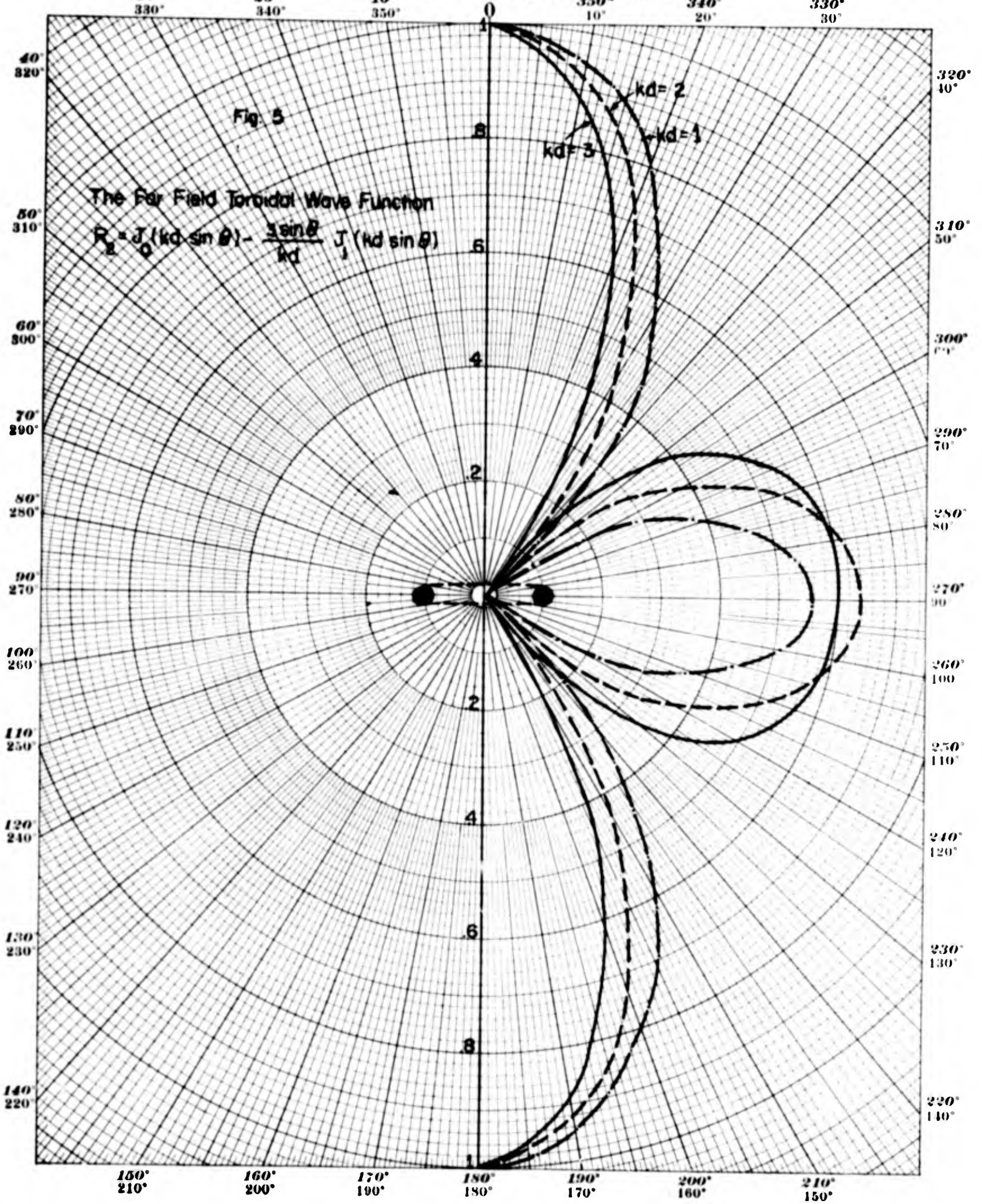

Parke Mathematical Laboratories - '64

Fig. 6

The Far Field Toroidal Wave Function

$$R_4 = J_0(kd\sin\theta) - \frac{10\sin\theta}{kd} J_1(kd\sin\theta) + \frac{35\sin^2\theta}{(kd)^2} J_2(kd\sin\theta)$$

kd = 1

kd = 2

kd = 3

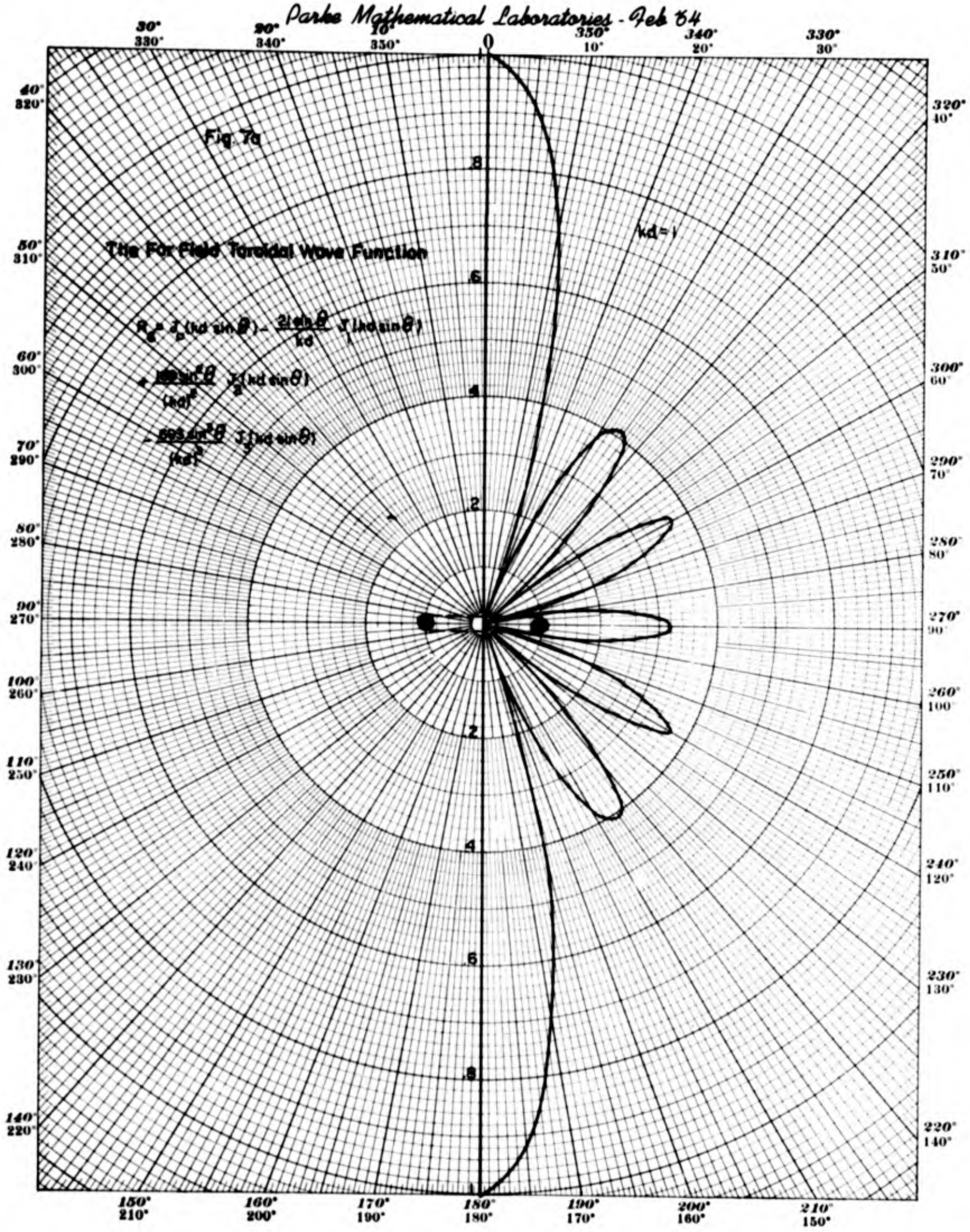
Parke Mathematical Laboratories - Feb 64
Fig 7a
The For Field Toroidal Wave Function
kd=1
30° 330°
20° 340°
10° 350°
0
350° 10°
340° 20°
330° 30°
40° 320°
50° 310°
60° 300°
70° 290°
80° 280°
90° 270°
100° 260°
110° 250°
120° 240°
130° 230°
140° 220°
320° 40°
310° 50°
300° 60°
290° 70°
280° 80°
270° 90°
260° 100°
250° 110°
240° 120°
230° 130°
220° 140°
.8
.6
.4
.2
.2
.4
.6
.8
150° 210°
160° 200°
170° 190°
180° 180°
190° 170°
200° 160°
210° 150°

Parke Mathematical Laboratories - '64

Fig. 7b

The Far Field Toroidal Wave Function

$$R_\theta = J_0(kd\sin\theta) - \frac{2i\sin\theta}{kd} J_1(kd\sin\theta) + \frac{i^2 3\sin^2\theta}{(kd)^2} J_2(kd\sin\theta) - \frac{i^3 3!\sin^3\theta}{(kd)^3} J_3(kd\sin\theta)$$

kd = 2

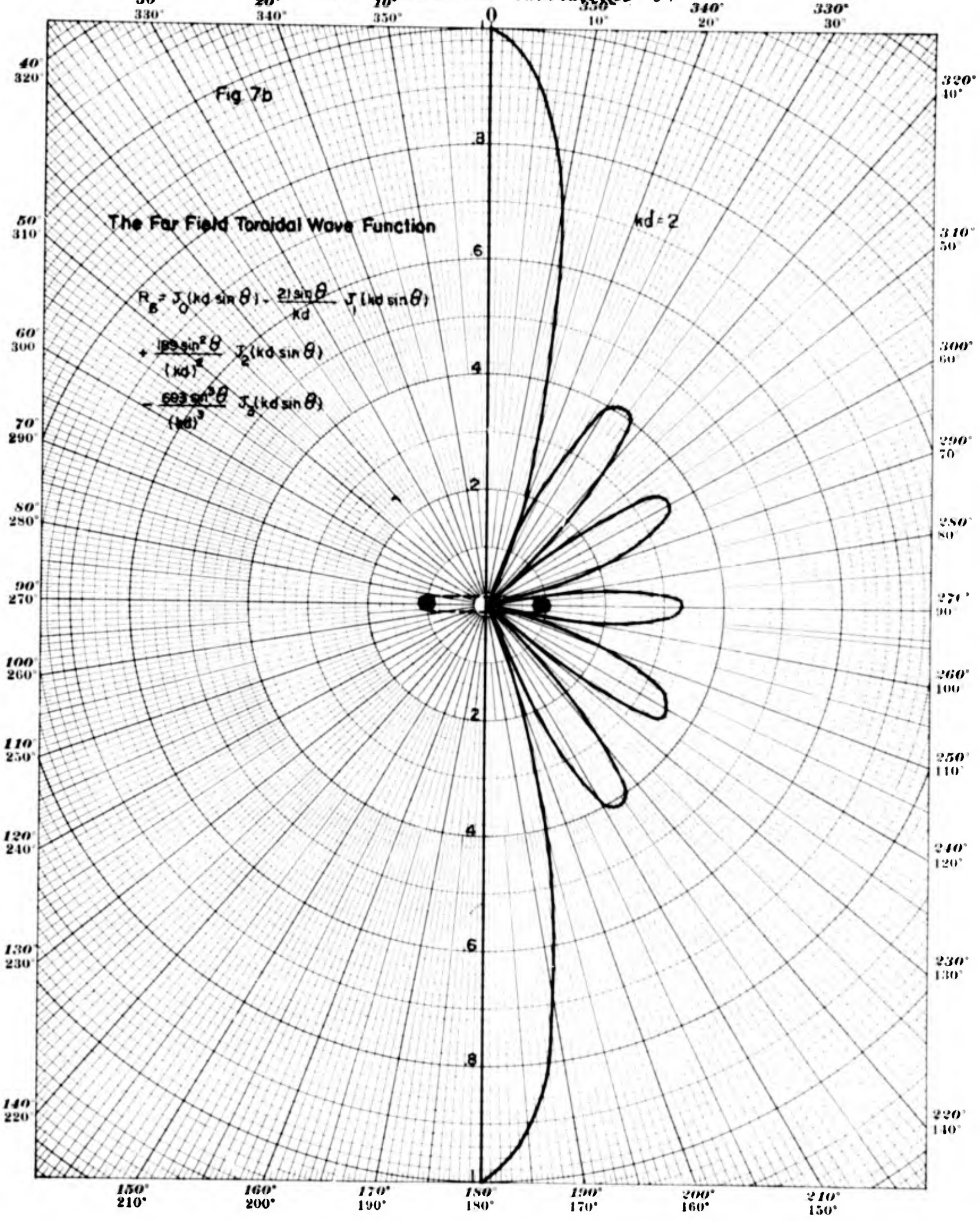

Parke Mathematical Laboratories - '64

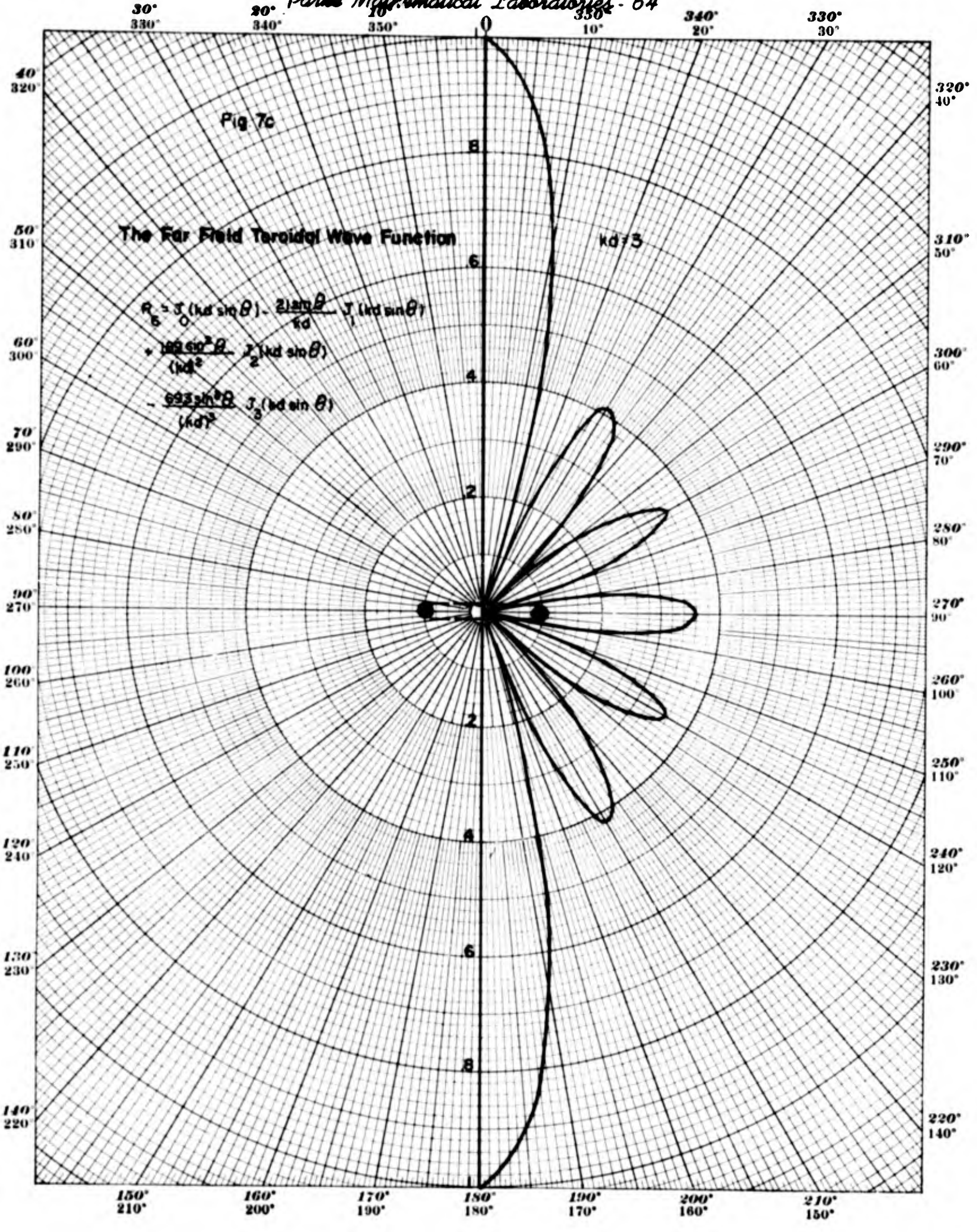

where $\epsilon_0 = 1/2$ and $\epsilon_\ell = 1$ for $\ell > 0$. This asymptotic form of $V_{2\ell}(s,\eta)$ has the same s and η dependence as the corresponding asymptotic form of the solution of Laplace's equation.[1] The two are basically different, however, because of the k dependence of $V_{2\ell}(s,\eta)$.

The value of the constant real part of $V_{2\ell}(s,\eta)$ as $s \to \infty$ was not given by Weston. However, it can be obtained as a power series in kd from the series representation in Eq. (6) for $N = 2\ell$ by using the asymptotic forms of the Legendre functions. Denoting this constant by $C_{2\ell}(kd)$ we find for $\ell = 0$ and $\ell = 1$:

$$C_0(kd) = \frac{1}{2}\sum_{p=0}^{\infty} \frac{(-1)^p}{(p!)^2(p+1/2)}(kd)^{2p},$$

$$C_2(kd) = \frac{1}{2}(kd)^2 \sum_{p=0}^{\infty} \frac{(-1)^p(p+1/2)}{p!(p+3/2)(p+5/2)\Gamma(p+3)}(kd)^{2p}$$

In Figures 8-10 the exact results for V_0, V_2 and V_4 for $s = 8$ and $kd = 1$ from Tables 2-4 are plotted as a function of η and compared with the corresponding asymptotic results as given by Eq. (15). The purpose of this comparison is to gain some idea of how large s must be to make Eq. (15) a useable approximation. We see that the exact and asymptotic functions have similar behaviour, but the values are often quite different. In Figures 11-13 a similar comparison is made of $\partial/\partial s\, V_{2\ell}(s,\eta)$. The exact values of this derivative were calculated from the integral

representation in connection with work in progress on radiation from a torus with relative cross sectional size corresponding to $s = 1$. The asymptotic real part of this derivative is zero, and the asymptotic imaginary part can be calculated from Eq. (15) (see next section of this report). The extent to which the exact and asymptotic derivatives agree is similar to that for the functions themselves. It appears that use of Eq. (15) must be confined to s considerably greater than 1 for most purposes.

Acoustic Radiation from a Thin Torus

General Solution

For the acoustic radiation problems which will have application to ring transducers the acoustic velocity potential can be taken as a linear combination of the $V_{2\ell}(s,\eta)$,

$$\Psi(s,\eta,t) = \psi(s,\eta)e^{-i\omega t} = e^{-i\omega t}\sum_{\ell=0}^{\infty} a_{2\ell} V_{2\ell}(s,\eta) , \tag{16}$$

where the expansion coefficients, $a_{2\ell}$, are chosen to satisfy the boundary conditions. In this case the boundary is the surface of a torus specified by $s = s_0$, and we are interested in Neumann conditions for which the normal derivative of $\psi(s,\eta)$ is specified on the boundary. We denote the normal velocity on the surface of the torus by

$$u(\eta,t) = U(\eta)e^{-i\omega t} , \tag{17}$$

and the outward normal derivative is given by

$$\frac{\partial\psi}{\partial n} = -\frac{1}{d}(s-\cos\eta)(s^2-1)^{1/2}\frac{\partial\psi}{\partial s} . \tag{18}$$

Fig. 8 The Toroidal Wave Function $V_{\phi}(s, \eta) = S_0 - i S_1$

kd = 1, s = 8

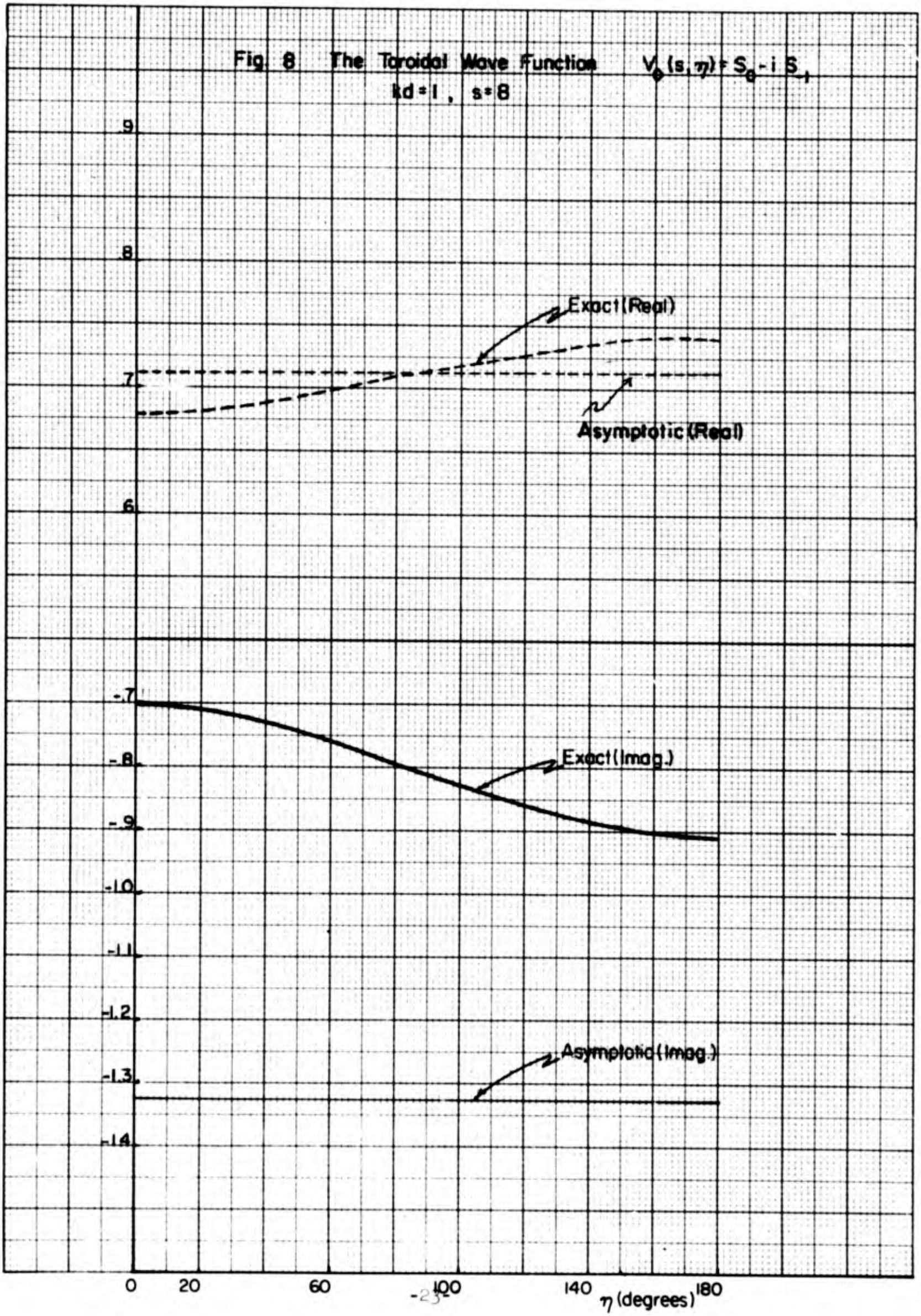

Fig. 9 The Toroidal Wave Function $V_2(s,\eta) = S_2 - i\,S_0$

$kd = 1$, $s = 8$

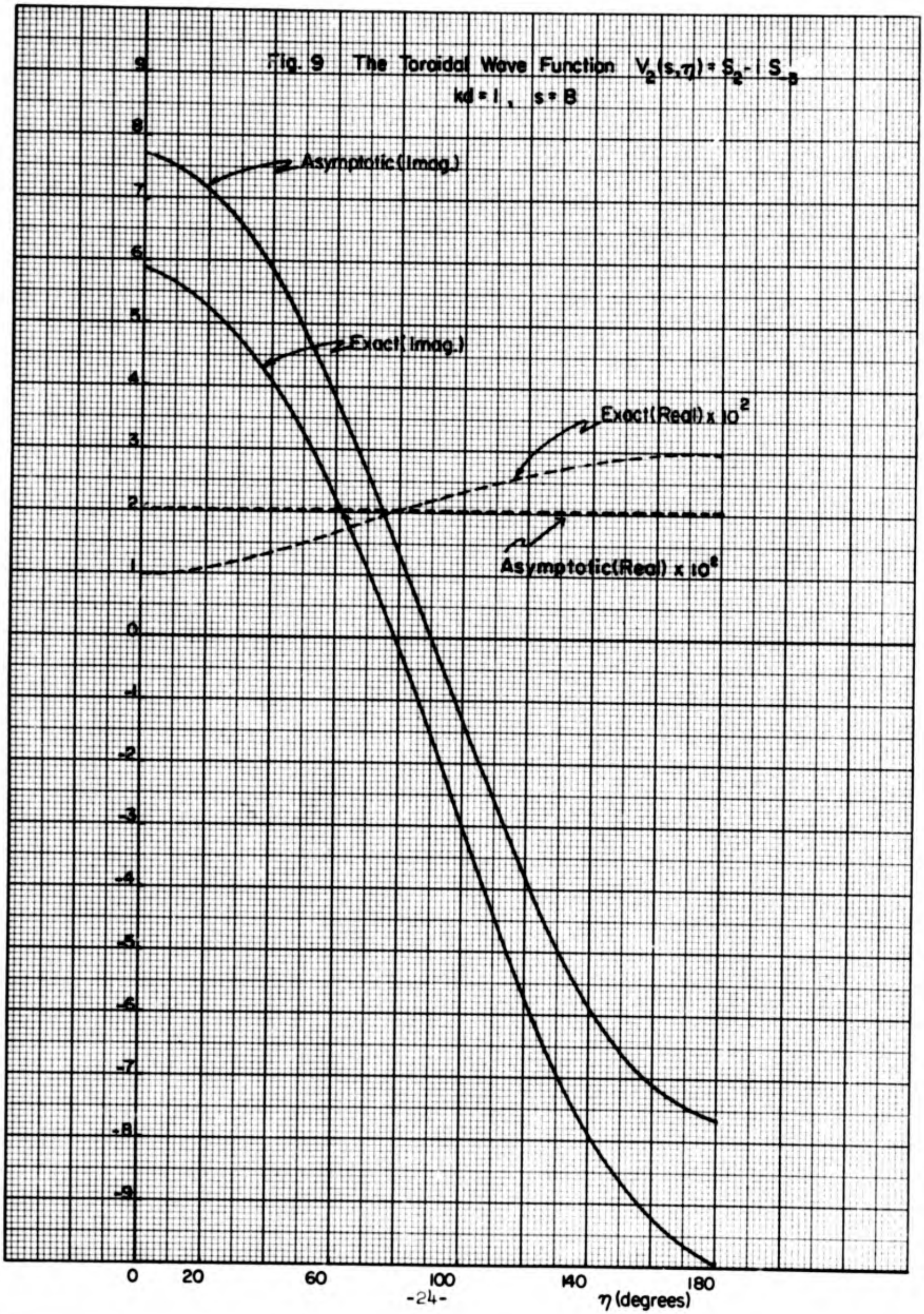

Fig.10 The Toroidal Wave Function $V_4(s,\eta) = S_4 - i\,S_{-5}$
$kd = 1,\ s = 8$

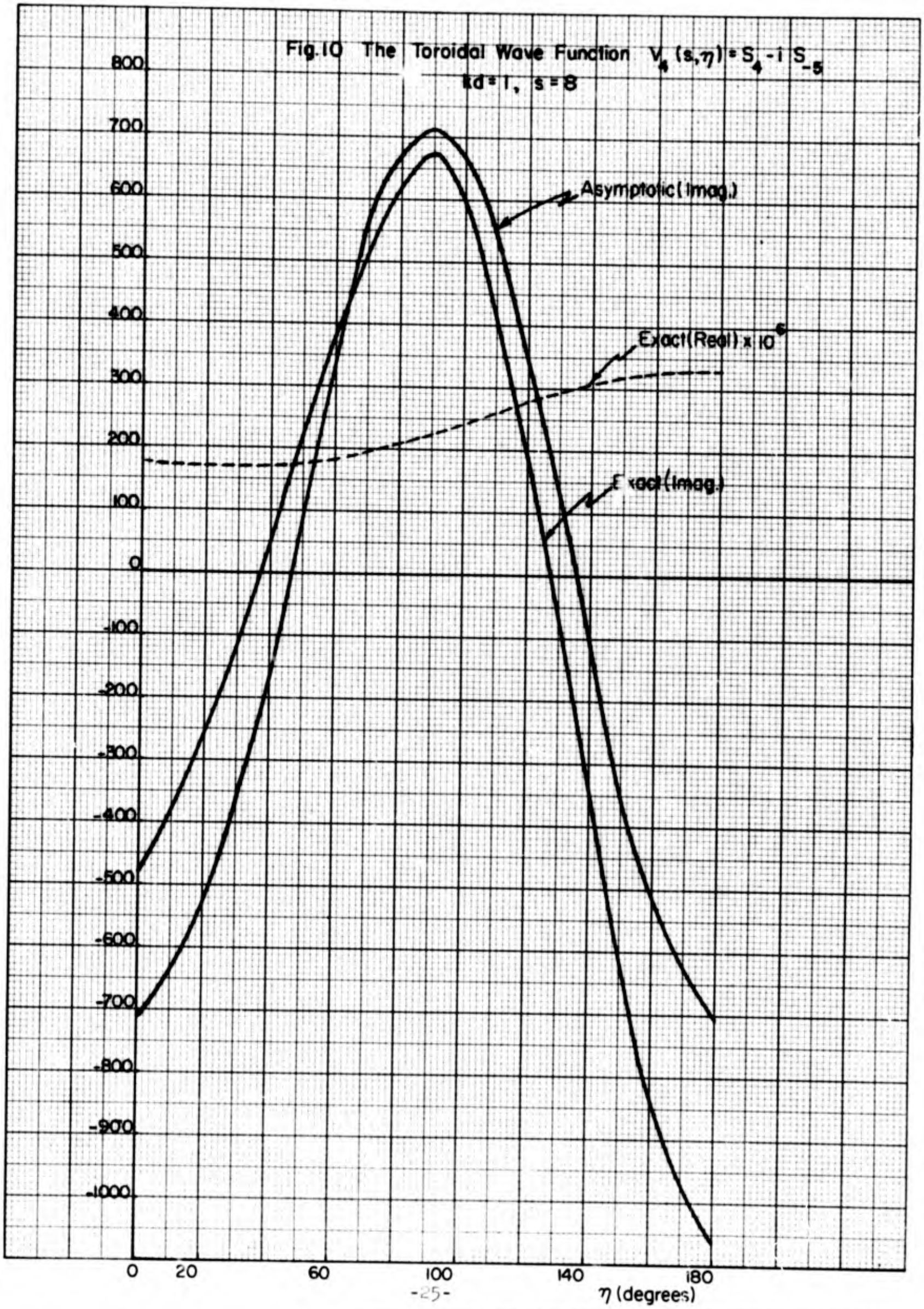

Fig. 11 $\frac{\partial}{\partial s} V_0(s,\eta)$

$kd = 1, \quad s = 8$

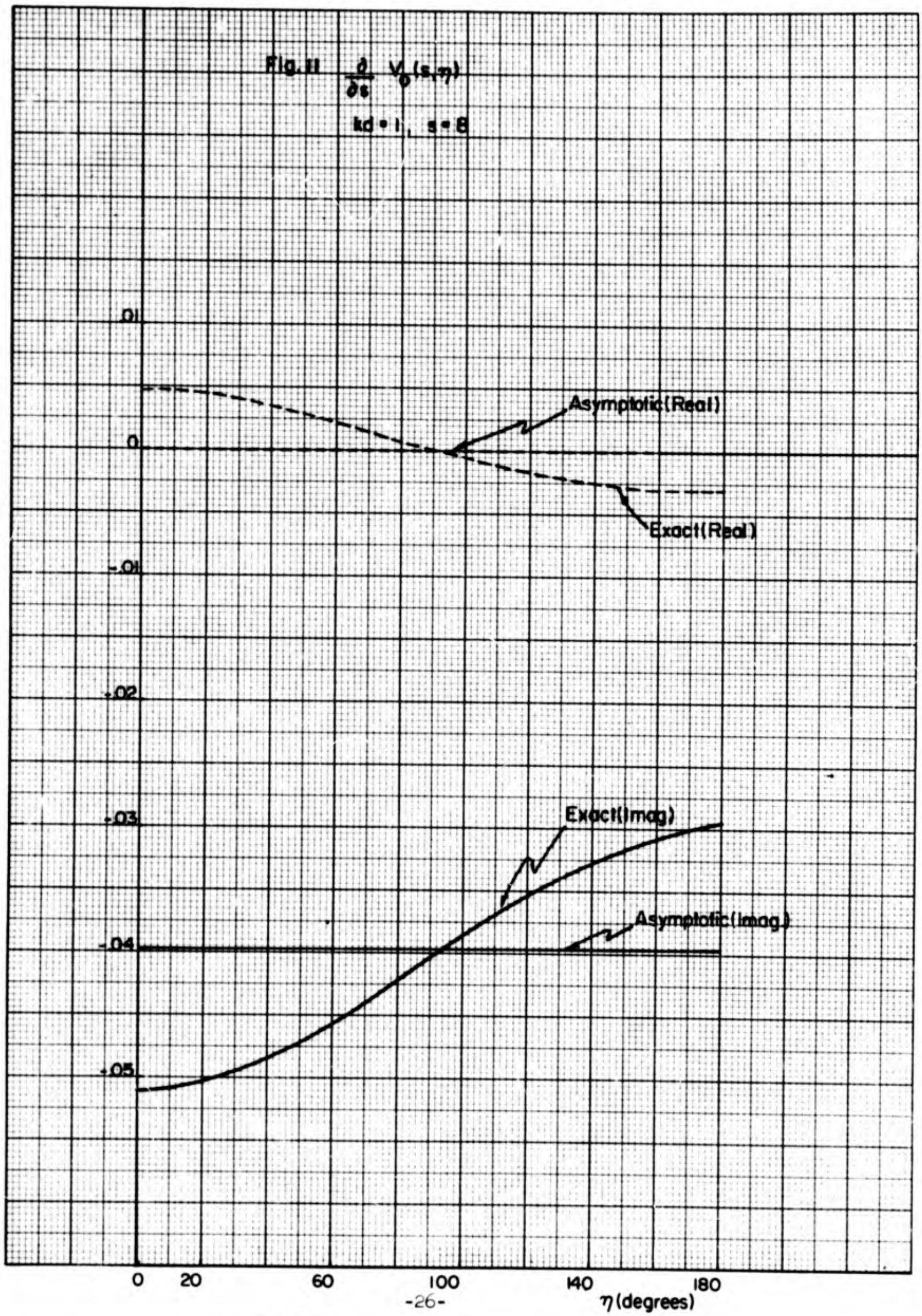

Fig. 12 $\frac{\partial}{\partial s} V_2(s,\eta)$

kd = 1, s = 8

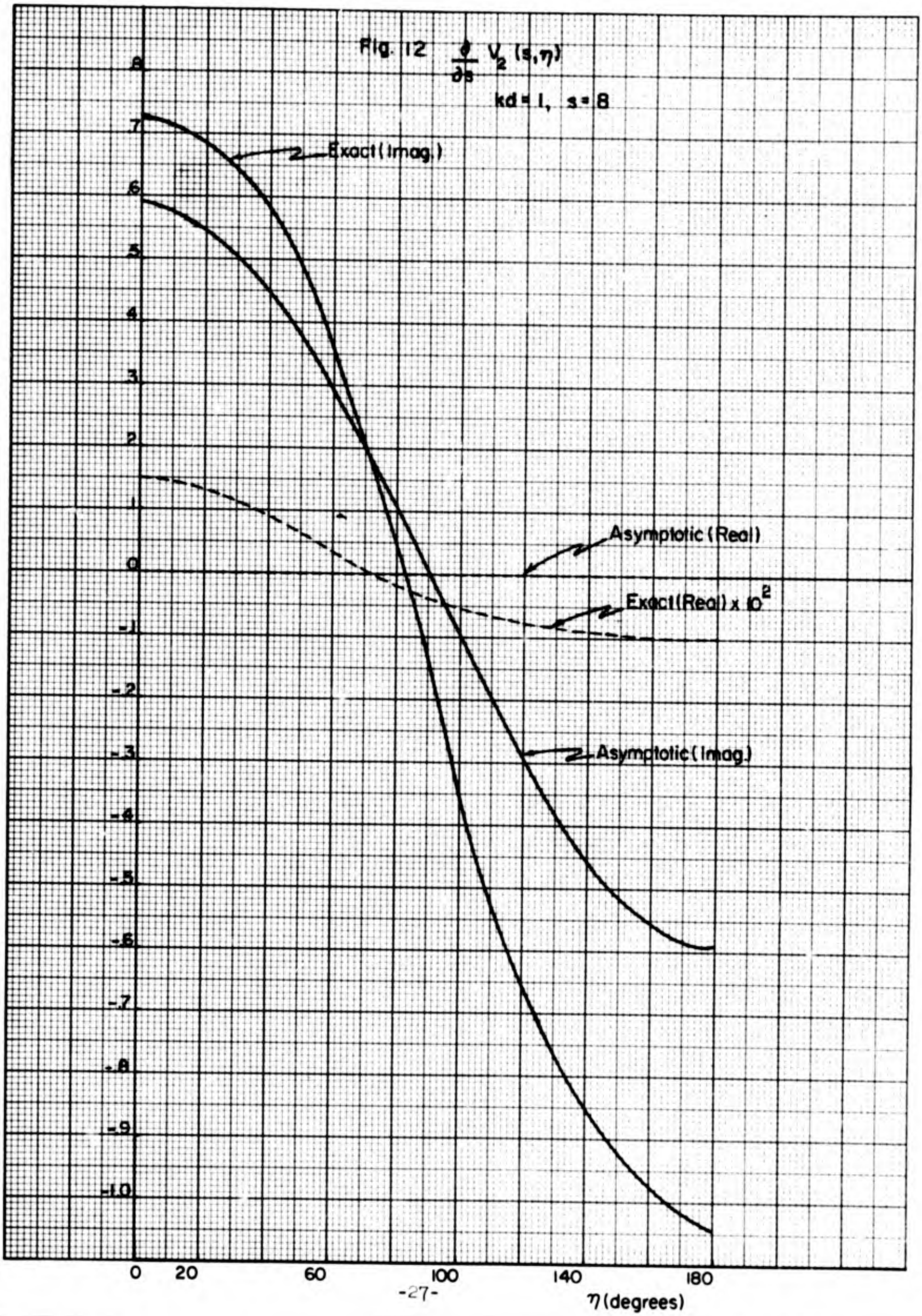

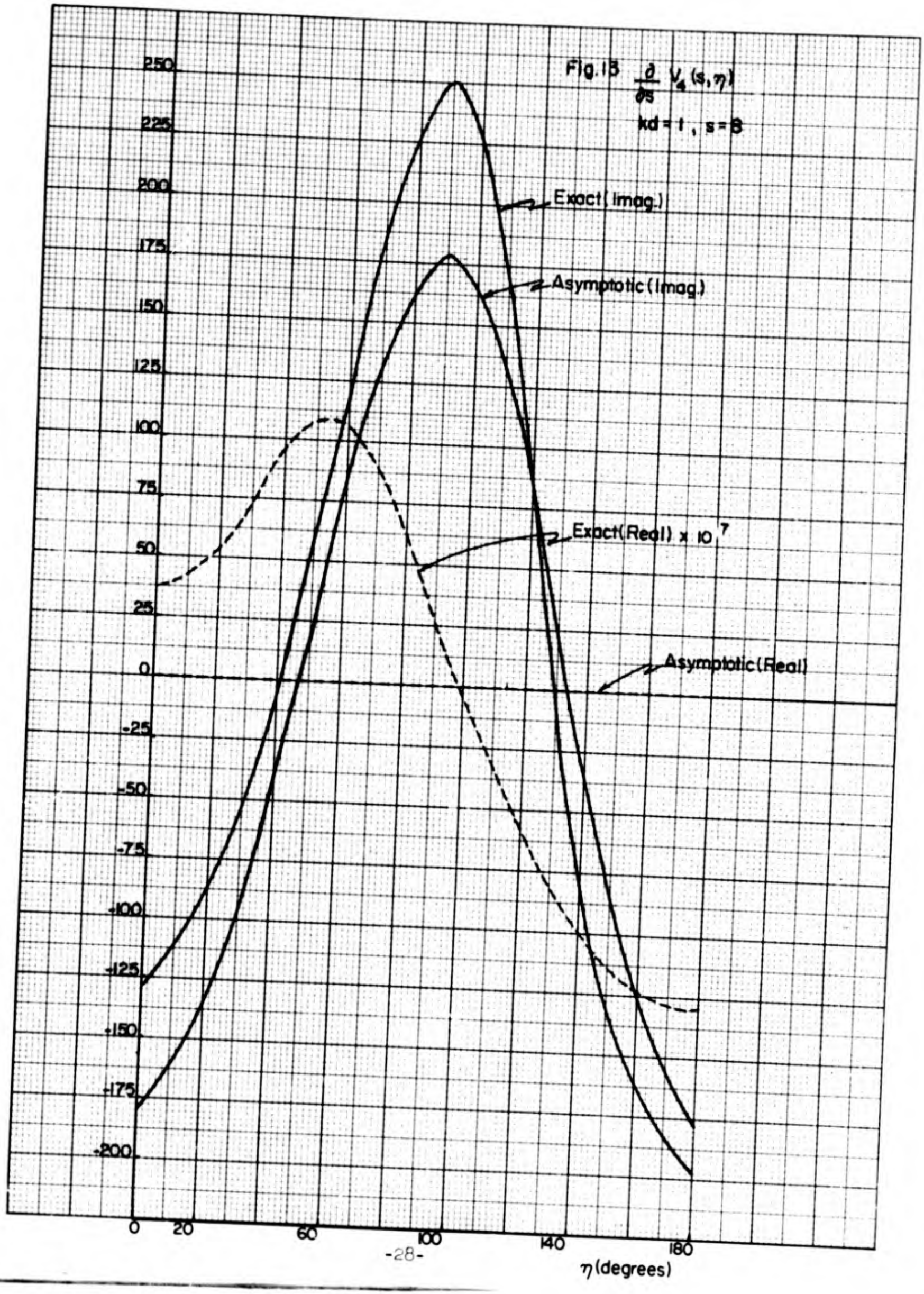
Fig. 13 $\frac{\partial}{\partial s} V_4(s,\eta)$
kd = 1 , s = 8
Exact(Imag.)
Asymptotic (Imag.)
Exact(Real) x 10^7
Asymptotic (Real)
250
225
200
175
150
125
100
75
50
25
0
-25
-50
-75
-100
-125
-150
-175
-200
0
20
60
100
140
180
η (degrees)

Combining these equations we find that the relation which determines the $a_{2\ell}$ is

$$-\frac{1}{d}(s_0 - \cos\eta\,\chi s_0^2 - 1)^{1/2} \sum_{\ell=0}^{\infty} a_{2\ell} \frac{\partial}{\partial s} V_{2\ell}(s,\eta)\Big|_{s=s_0} = U(\eta). \tag{19}$$

There is no known weight function with respect to which the functions $V_{2\ell}(s_0,\eta)$ or $\partial/\partial s\, V_{2\ell}(s,\eta)\big|_{s=s_0}$ are orthogonal in general (3, p. 256). The general torus problem then involves all the technical complications of determining the expansion coefficients in the case of non-orthogonal functions. The details of these technicalities have been described before,[11] and are being used in the other problems mentioned in the introduction. The remainder of this report will be devoted to the case $s_0 \to \infty$ where we can use Eq. (15) in Eq. (19) to satisfy the boundary conditions. The important characteristic of Eq. (15) is that the asymptotic $\partial/\partial s\, V_{2\ell}(s,\eta)\big|_{s=s_0}$ are orthogonal functions of η with respect to any constant weight factor, because they are proportional to $\cos \ell\eta$. Thus in this special case we can determine the $a_{2\ell}$ by relatively simple procedures. Note that we are using the asymptotic wave functions only to satisfy the boundary conditions; once the $a_{2\ell}$ have been determined they can be used in Eq. (16) with the general wave functions. For example, we will find that this solution is most useful in the far field.

The case $s_0 \to \infty$, which corresponds to $R_1 \to 0$ and $R_2 \to d$, means that we are considering the problem of radiation from a torus with infinitesimally thin cross section. We must expect this problem to have limited usefulness as a mathematical model for ring transducers, since the

only feature which might make it a good model is its appropriate topology. We will find, however, that when a suitable velocity distribution is chosen the thin torus gives us a rather good model for the far field.

After writing Eq. (19) for $s_0 \to \infty$ and using Eq. (15) we have

$$\frac{s_0^2\sqrt{2\pi}}{id}\sum_{\ell=0}^{\infty} a_{2\ell}\,\frac{(-1)^{\ell+1}\epsilon_\ell\,\bar{F}_{2\ell}(s_0)}{(kd)^{2\ell+1}\Gamma(\frac{1}{2}-2\ell)}\cos\ell\eta = U(\eta), \tag{20}$$

where we have used the abbreviation

$$F_{2\ell}(s_0) = \partial/\partial s\left[s^{1/2}P_{\ell-1/2}(s)\right]\Big|_{s=s_0\to\infty}. \tag{21}$$

Any $U(\eta)$ of the type under consideration can be expanded in a Fourier cosine series,

$$U(\eta) = \sum_{\ell=0}^{\infty} U_\ell \cos\ell\eta, \tag{22}$$

and then comparison with Eq. (20) gives

$$a_{2\ell} = \frac{id(kd)^{2\ell+1}\Gamma(\frac{1}{2}-2\ell)}{s_0^2\sqrt{2\pi}\,(-1)^{\ell+1}\epsilon_\ell F_{2\ell}(s_0)}\,U_\ell. \tag{23}$$

After carrying out the indicated differentiation in Eq. (21) we have

$$\partial/\partial s\left[s^{1/2}P_{\ell-1/2}(s)\right]\Big|_{s=s_0} = \frac{1}{s_0^2-1}\left[s_0^{1/2}(\ell+1/2)P_{\ell+1/2}(s_0) - \frac{(2\ell s_0^2+1)}{2s_0^{1/2}}P_{\ell-1/2}(s_0)\right].$$

The asymptotic forms of the Legendre functions are (3, p. 255)

$$\left.\begin{aligned} P_{-1/2}(s_0) &\to \frac{1}{\pi}\sqrt{\frac{2}{s_0}}\left[\ln(2s_0) + \text{constant}\right] \\ P_\nu(s_0) &\to \frac{(2s_0)^\nu\Gamma(\nu+1/2)}{\pi^{1/2}\Gamma(\nu+1)}, \quad \nu > -1/2 \end{aligned}\right\} s_0\to\infty$$

with which we find

$$\left.\begin{aligned} F_0(s_0) &= \frac{\sqrt{2}}{\pi s_0} \\ F_{2\ell}(s_0) &= \frac{s_0^{\ell-1}\, 2^{\ell-1/2}}{\pi^{1/2}} \frac{\Gamma(\ell+1)}{\Gamma(\ell+1/2)}, \quad \ell > 0 \end{aligned}\right\}$$

Putting these results into Eq. (23) we have

$$a_{2\ell} = \frac{id\,(kd)^{2\ell+1}\,\Gamma(\tfrac{1}{2}-2\ell)\,\Gamma(\ell+1/2)}{s_0^{\ell+1}\,2^{\ell}(-1)^{\ell+1}\,\Gamma(\ell+1)}\, U_\ell , \tag{24}$$

as the general expression for the expansion coefficients for the sound field of a thin torus with a normal velocity distribution of the type in Eq. (22).

In carrying out the solution of this vanishingly thin torus problem it is necessary to use, in Eq. (19), the asymptotic normal derivatives of the toroidal wave functions. It is not obvious that the procedure above accomplishes this, because we have differentiated the asymptotic wave functions instead of finding the asymptotic derivatives. This point has been investigated by differentiating the series representations of the wave functions, multiplying by $\left[-\frac{1}{d}(s-\cos\eta)(s^2-1)^{1/2}\right]$, and then taking the limit as $s \to \infty$. It was shown in this way that the procedure described above does give the correct results.

An Approximate Solution for Ring Transducers

We assume that at frequencies near the fundamental ring resonance

the motion of a ring transducer is mainly an alternating increase and decrease of the mean radius R_2 for which the velocity can be written

$$\frac{\delta R_2}{\delta t} = U_1 e^{-i\omega t} \tag{25}$$

However, this motion is necessarily accompanied by a Poisson contraction and expansion of the cross section. For a torus this part of the motion can be considered as an alternating increase and decrease of the cross section radius R_1, and the corresponding velocity can be written

$$\frac{\delta R_1}{\delta t} = U_0 e^{-i\omega t} \tag{26}$$

Actual ring transducers are usually driven either by electrostriction or magnetostriction, and a detailed description of the motion would have to include these effects. For the present, however, we will assume that the motion can be usefully approximated by a superposition of the simple motions in Eqs. (25) and (26).

$\delta R_1/\delta t$ is normal to the surface of the torus, but $\delta R_2/\delta t$ is a purely radial motion which has the Cartesian components

$$u_x = U_1 \cos\varphi \; e^{-i\omega t},$$
$$u_y = U_1 \sin\varphi \; e^{-i\omega t},$$
$$u_z = 0,$$

for the z-axis along the axis of the torus. When this vector is transformed to toroidal coordinates we find for the s component, which is normal to the surface of the torus,

$$u_s = U_1 e^{-i\omega t} \; \frac{s_0 \cos\eta - 1}{s_0 - \cos\eta} .$$

With these results our normal velocity distribution is

$$U(\eta) = U_0 + U_1 \frac{s_0 \cos\eta - 1}{s_0 - \cos\eta} . \tag{27}$$

Since the two motions which have been superimposed are Poisson coupled the amplitude constants U_0 and U_1 are related. We can evaluate one in terms of the other by satisfying the physically reasonable requirement that for a thin torus the motion we have chosen corresponds to relative volume changes which are the same as those for a straight, thin rod when its length is changed. For a rod of length ℓ the volume velocity is related to the longitudinal velocity by

$$\frac{\delta V}{\delta t} = \frac{V}{\ell} \frac{\delta \ell}{\delta t} (1 - 2\sigma), \tag{28}$$

where σ is Poisson's ratio. For the thin torus we therefore want

$$\frac{\delta V}{\delta t} = \frac{V}{R_2} \frac{\delta R_2}{\delta t} (1 - 2\sigma). \tag{29}$$

Since the volume of a torus is $2\pi^2 R_2 R_1^2$, we have

$$\frac{\delta V}{\delta t} = \frac{2V}{R_1} \frac{\delta R_1}{\delta t} + \frac{V}{R_2} \frac{\delta R_2}{\delta t} = \left(\frac{2V}{R_1} U_0 + \frac{V}{R_2} U_1 \right) e^{-i\omega t}, \tag{30}$$

and equating Eqs. (29) and (30) gives

$$U_0 = - \frac{R_1 \sigma}{R_2} U_1 = - \frac{\sigma}{s_0} U_1 , \tag{31}$$

where we have used $s_0 = R_2/R_1$ as shown in the Appendix.

Using Eq. (31) in Eq. (27) our approximate velocity distribution becomes

$$U(\eta) = U_1 \left[- \frac{\sigma}{s_0} + \frac{s_0 \cos\eta - 1}{s_0 - \cos\eta} \right]. \tag{32}$$

We can put $U(\eta)$ in the form of Eq. (22) by expanding the second term in Eq. (32). Keeping terms only to order $1/s_0$ [to be consistent with the first term of Eq. (32)] we have

$$U(\eta) = U_1\left[-\frac{\sigma}{s_0} - \frac{1}{2s_0} + \cos\eta + \frac{\cos 2\eta}{2s_0} + \cdots\right]. \tag{33}$$

This is in the form of Eq. (22) with

$$U_0 = -\frac{U_1}{s_0}(\sigma + 1/2),$$

$$U_1 = U_1,$$

$$U_2 = U_1/2s_0,$$

and from Eq. (24) we find

$$a_0 = \frac{id\,kd\,\pi(\sigma+1/2)}{s_0^2}\,U_1, \tag{34}$$

$$a_2 = \frac{id\,(kd)^3\,\pi}{3s_0^2}\,U_1. \tag{35}$$

We note that both these coefficients are proportional to U_1/s_0^2. For the limiting problem of $s_0 \to \infty$ we must also imagine $U_1 \to \infty$ such that U_1/s_0^2 remains finite. This corresponds to keeping the volume velocity (or source strength) finite. When we use $U_2 = U_1/2s_0$ in Eq. (24) we find a_4 proportional to U_1/s_0^4 which vanishes in the limit compared to a_0 and a_2. In the same way all higher order coefficients vanish.

With these values for a_0 and a_2 we have for the spatial part of the velocity potential for a thin torus with the normal velocity distribution in Eq. (32)

$$\psi(s,\eta) = \frac{id\,kd\,\pi\,U_1}{s_0^2}\left[(\sigma+1/2)V_0(s,\eta) + \frac{1}{3}(kd)^2 V_2(s,\eta)\right], \tag{36}$$

and the corresponding result for the sound pressure is

$$p(s,\eta,t) = i k\rho c\, \psi(s,\eta) e^{-i\omega t} = -\pi\rho c\, U_1 \left(\frac{kd}{s_0}\right)^2 e^{-i\omega t}\left[(\sigma+\tfrac{1}{2})V_0(s,\eta) + \tfrac{1}{3}(kd)^2 V_2(s,\eta)\right]. \qquad (37)$$

Eq. (37) is the final result of our attempt to obtain a useful mathematical model for the ring transducer based on the results of the thin torus problem obtained in the last section. We must not overlook the distinction between the thin torus problem, which is solved exactly by Eq. (24), and the ring transducer problem, for which Eq. (37) may be a useful approximation. The remainder of this report will be concerned with a detailed investigation of special features of Eq. (37) which can help to determine its usefulness.

Comparison with Far Field Measurements

During the years of development work with free-flooding ring transducers there have been many measurements of far field patterns as well as some near field measurements. However, there seem to be few cases in which the measurements were carried out under sufficiently well controlled conditions to provide data suitable for comparison with theoretical calculations. Qualitatively it has been found that the main features of ring transducer far field patterns near ring resonance consist of a maximum in the plane of the ring and a minimum, or sometimes a minor lobe, along the axis of the ring.

The far field case of our theoretical result in Eq. (37) is obtained by use of Eq. (13). We get

$$p(r,\theta,t) = i\pi\rho c\, U_1 \left(\frac{kd}{s_0}\right)^2 \frac{e^{-i(\omega t - kr)}}{kr}\left[(\sigma+\tfrac{1}{2})R_0(\cos\theta) - \tfrac{1}{3}(kd)^2 R_2(\cos\theta)\right], \qquad (38)$$
$$r \to \infty,$$

where the functions $R_0(\cos\theta)$ and $R_2(\cos\theta)$ are plotted in Figures 4 and 5 for typical values of kd. For comparison with this result we have chosen patterns published by McMahon.[12] The transducer used for McMahon's Fig. 3 has $R_2 = 1.76$ cm, and the height and wall thickness are such that we find $R_1 = 0.37$ cm for equal area circular cross section. These dimensions give $d = 1.72$ cm (see relations in Appendix). At the ring resonance ($26\,kc$) we then have $kd = 1.87$ and at cavity resonance ($18\,kc$) $kd = 1.29$.

Figures 14a and 14b compare McMahon's measurements with the pressure amplitude calculated from Eq. (38), using $\sigma = 0.3$ and normalizing to unity in the plane of the ring ($\theta = 90^\circ$). At the ring resonance (Fig. 14a) we find good agreement between the measured and calculated patterns. At the cavity resonance (Fig. 14b) the agreement is poorer, which is reasonable since the velocity distribution chosen was expected to be a good approximation only near ring resonance.

It appears that our basic theoretical result contains at least the essential features of the far field of ring transducers near ring resonance. Far field pressure amplitude patterns calculated from Eq. (38) are illustrated further in Fig. 15 for $kd = 1$, 2, and 3. Ring transducers are usually made of materials such that, when mass loaded by vibrating in water, the value of kR_2 (which is approximately the same as kd) is about two. We see from Fig. 15 that it is near $kd = 2$ that the two terms in Eq. (38) combine to give a null or a small minor lobe along the axis as is observed. This emphasizes the significance of the fact that the velocity

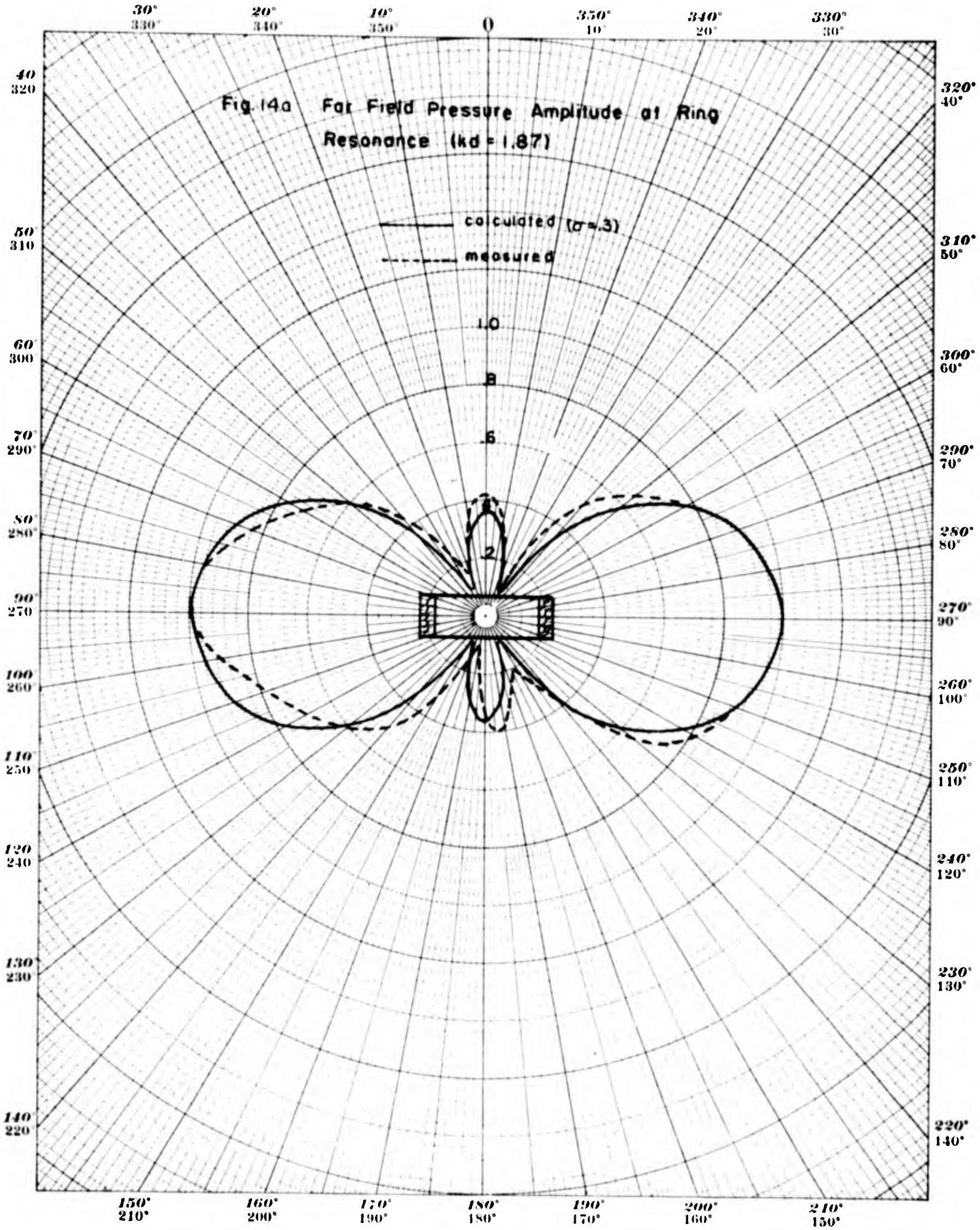
Fig. 14a Far Field Pressure Amplitude at Ring Resonance (kd = 1.87)
calculated (σ=.3)
measured
1.0
.8
.6
.4
.2
30° 330°
20° 340°
10° 350°
0
350° 10°
340° 20°
330° 30°
40° 320°
50° 310°
60° 300°
70° 290°
80° 280°
90° 270°
100° 260°
110° 250°
120° 240°
130° 230°
140° 220°
320° 40°
310° 50°
300° 60°
290° 70°
280° 80°
270° 90°
260° 100°
250° 110°
240° 120°
230° 130°
220° 140°
150° 210°
160° 200°
170° 190°
180° 180°
190° 170°
200° 160°
210° 150°

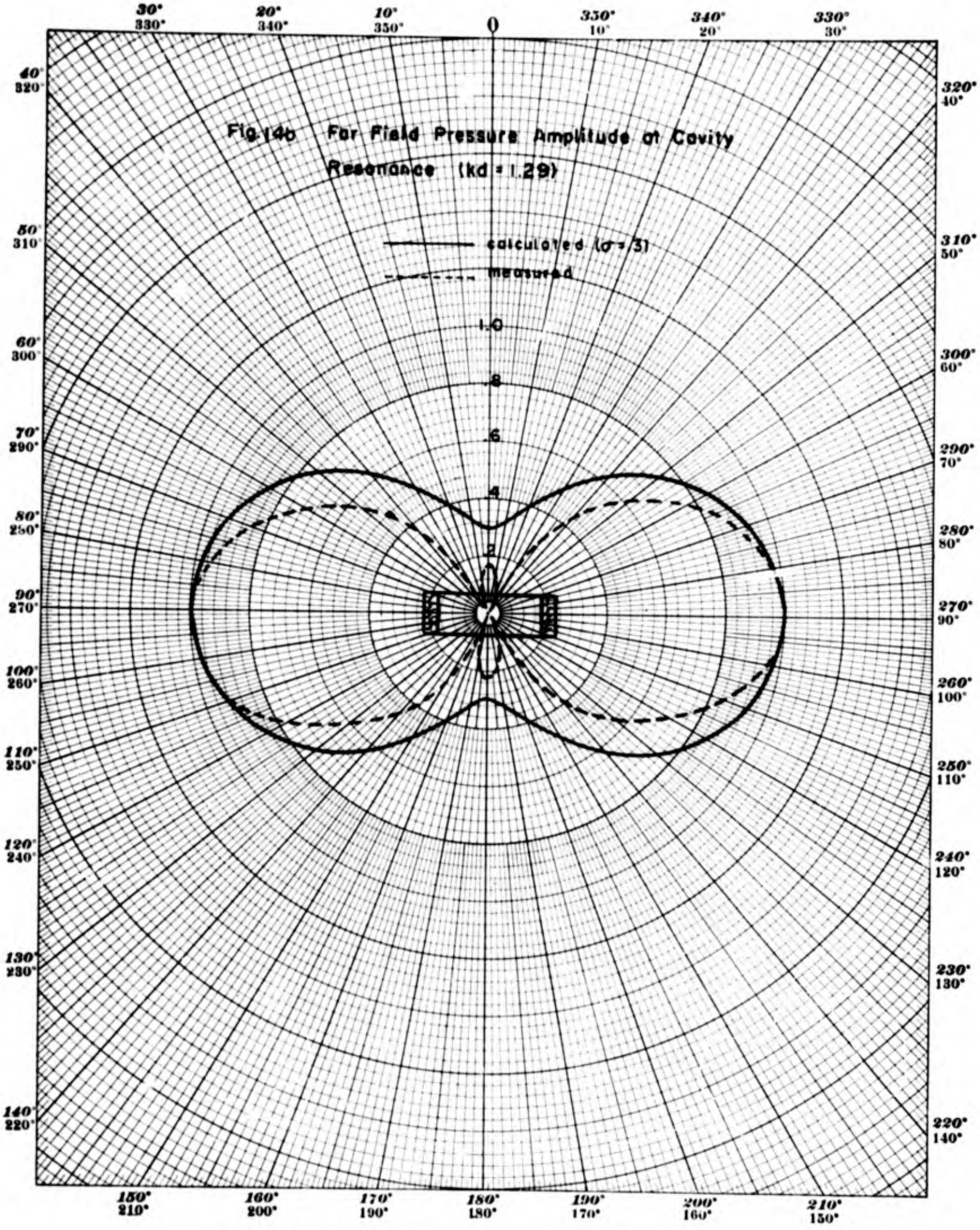
Fig 14b Far Field Pressure Amplitude at Cavity Resonance (kd = 1.29)
calculated (σ = 3)
measured
1.0
.8
.6
.4
.2
0
30° 330°
20° 340°
10° 350°
350° 10°
340° 20°
330° 30°
40° 320°
50° 310°
60° 300°
70° 290°
80° 280°
90° 270°
100° 260°
110° 250°
120° 240°
130° 230°
140° 220°
320° 40°
310° 50°
300° 60°
290° 70°
280° 80°
270° 90°
260° 100°
250° 110°
240° 120°
230° 130°
220° 140°
150° 210°
160° 200°
170° 190°
180° 180°
190° 170°
200° 160°
210° 150°

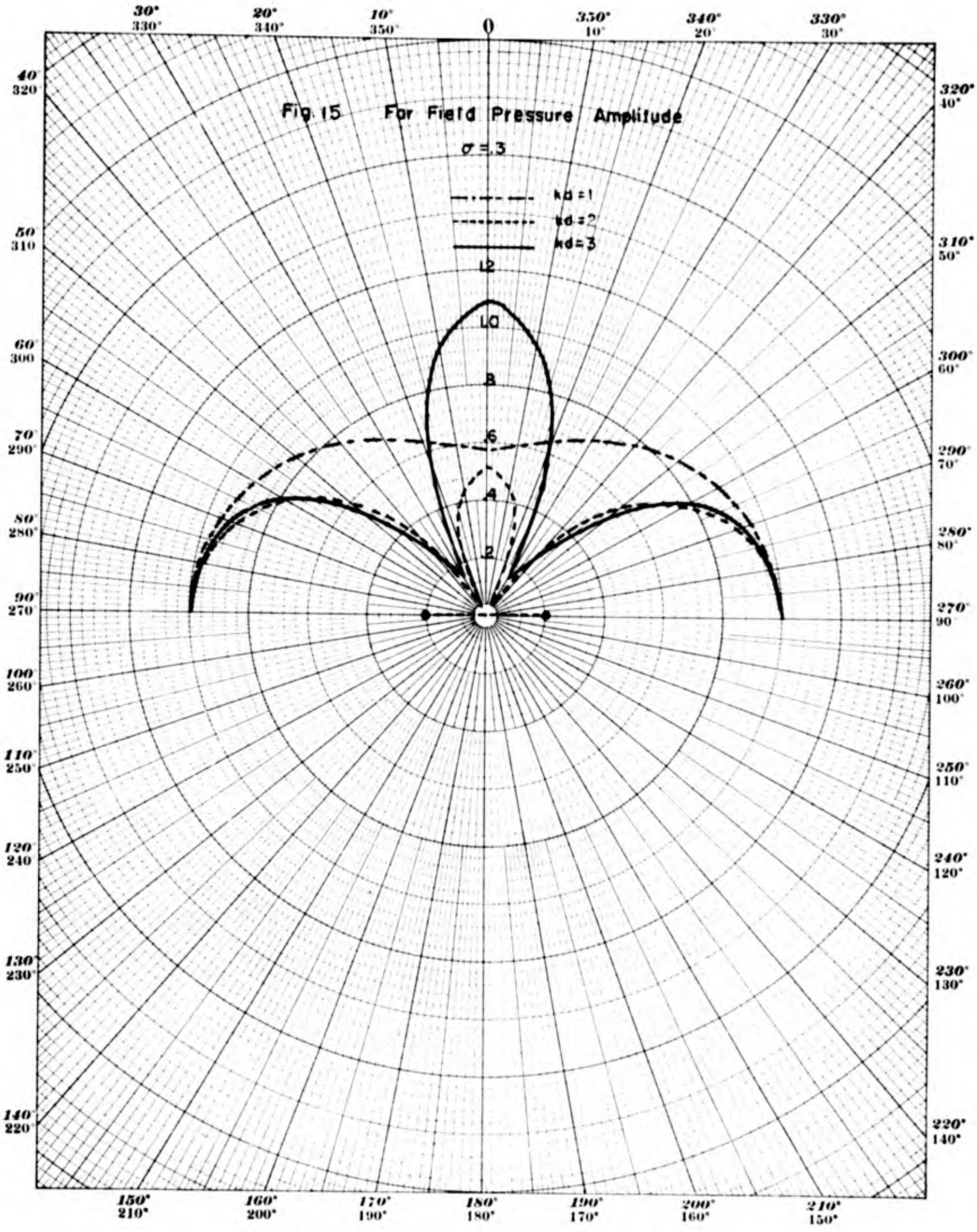
Fig. 15 For Field Pressure Amplitude
σ = .3
ka = 1
ka = 2
ka = 3
12
10
8
6
4
2
0
30° 330°
20° 340°
10° 350°
350° 10°
340° 20°
330° 30°
40° 320°
50° 310°
60° 300°
70° 290°
80° 280°
90° 270°
100° 260°
110° 250°
120° 240°
130° 230°
140° 220°
320° 40°
310° 50°
300° 60°
290° 70°
280° 80°
270° 90°
260° 100°
250° 110°
240° 120°
230° 130°
220° 140°
150° 210°
160° 200°
170° 190°
180° 180°
190° 170°
200° 160°
210° 150°

distribution in Eq. (32) leads to both a_0 and a_2 remaining in the limit and having about the same magnitude at $kd \approx 2$. Both terms are required to get a null or a small minor lobe along the axis.

The Sound Field Near the Torus and the Radiation Reactance

In a small toroidal region near the thin torus the sound field can be described approximately by using the asymptotic wave functions in Eq. (15). This, however, only gives a consistent approximation for the imaginary part of the pressure which is the dominant part in this region. The constant real parts of the asymptotic wave functions played no role in evaluating the expansion coefficients, and their use now would correspond to keeping terms of the same size as others which have been neglected. Thus in this region near the torus the pressure is 90° out of phase with $U_1 e^{-i\omega t}$ and is given by

$$p(s,\eta,t) \approx i\pi\rho c U_1 \left(\frac{kd}{s_0}\right)^2 e^{-i\omega t}\left[(\sigma+1/2)\frac{s^{1/2}P_{-1/2}(s)}{\sqrt{2}\,kd} - \frac{s^{1/2}P_{1/2}(s)}{2\sqrt{2}\,kd}\cos\eta\right]. \quad (39)$$

These phase relations are characteristic of the pressure on the surface of the source for any vanishingly small source. In such cases the power and the radiation resistance must be calculated from the far field, but the near field expressions, such as Eq. (39), can be used to calculate the radiation reactance.

When referred to U_1 the radiation reactance is given by

$$X_{11} = -\mathrm{Im}\left\{\frac{1}{U_1^2}\iint p(s_0,\eta,t)\,u^*(\eta,t)\,dS\right\}, \quad (40)$$

where dS is the differential area element on a torus which is given by

$$dS = \frac{d^2 (s_0^2 - 1)^{1/2}}{(s_0 - \cos\eta)^2} \, d\eta \, d\varphi \xrightarrow[s_0 \to \infty]{} \frac{d^2}{s_0} \, d\eta \, d\varphi .$$

Using

$$u(\eta, t) = U_1 e^{-i\omega t} \left[-\frac{1}{s_0} (\sigma + 1/2) + \cos\eta \right],$$

carrying out the integration, and using the asymptotic forms of the Legendre functions for $s_0 \to \infty$ we find

$$X_{11} = \frac{2\pi^2 d^2 \rho c \, kd}{s_0^2} . \tag{41}$$

The expression for the radiation reactance in Eq. (41) is such that the ratio of the radiation mass, $m_r = X_{11}/\omega$, to the mass of the torus, m_T, is finite in the limit and has the value

$$m_r / m_T = \rho / \rho_T ,$$

where ρ_T is the density of the torus material. For typical densities of electrostrictive or magnetostrictive materials this ratio corresponds to a decrease of the resonant frequency by 5-10% due to mass loading by water, while measurements on ring transducers usually show a greater decrease of the resonant frequency However, it is not surprising that the radiation reactance for the infinitesimally thin torus fails to correspond to observations on ring transducers. The radiation reactance is strongly dependent on the near field and on the detailed shape of the source.

The Radiation Resistance and Directivity Index

The radiation resistance for a thin torus can be obtained by calculating the radiated power from the far field expression for the pressure. If the

radiation resistance is referred to U_1 the time average radiated power can be written

$$\bar{P} = \tfrac{1}{2} R_{11} U_1^2, \tag{42}$$

where R_{11} is the self radiation resistance. The power can be calculated by integrating the time average far field intensity over all directions

$$\bar{P} = 2\pi \int_0^\pi \frac{p p^*}{2\rho c} r^2 \sin\theta \, d\theta. \tag{43}$$

Using Eq. (38) for he pressure and equating the two expressions for $\bar{P}$ we find

$$R_{11} = \frac{2\pi^3 \rho c}{k^2} \left(\frac{kd}{s_0}\right)^4 \int_0^\pi \left[(\sigma + \tfrac{1}{2}) R_0(\cos\theta) - \tfrac{1}{3}(kd)^2 R_2(\cos\theta)\right]^2 \sin\theta \, d\theta \tag{44}$$

Using Eq. (14) for the far field toroidal functions and the series representations for the Bessel functions we have

$$\left[(\sigma + \tfrac{1}{2}) R_0(\cos\theta) - \tfrac{1}{3}(kd)^2 R_2(\cos\theta)\right] = \sum_{n=0}^{\infty} \frac{(-1)^n}{(n!)^2} \left(\frac{kd \sin\theta}{2}\right)^{2n} (B_0 - 2n),$$

where $$B_0 = \sigma + \frac{1}{2} - \frac{1}{3}(kd)^2.$$

When this series is squared and the integration in Eq. (44) is carried out we find

$$R_{11} = \frac{2\pi^3 \rho c \sqrt{\pi}}{k^2} \left(\frac{kd}{s_0}\right)^4 \sum_{n=0}^{\infty} \sum_{m=0}^{\infty} \frac{(-1)^{n+m}}{(n!)^2 (m!)^2} \left(\frac{kd}{2}\right)^{2n+2m} (B_0 - 2n)(B_0 - 2m) \frac{\Gamma(m+n+1)}{\Gamma(m+n+3/2)}.$$

By use of $$\Gamma(n+1/2) = \frac{\sqrt{\pi}}{2^n} (2n-1)!!,$$

where $$(2n-1)!! = (2n-1)(2n-3) \cdots 3 \cdot 1,$$

the expression for R_{11} can be written

$$R_{11} = \frac{2\pi^3 \rho c}{k^2} \left(\frac{kd}{s_0}\right)^4 \sum_{n=0}^{\infty} \sum_{m=0}^{\infty} \frac{(-1)^{n+m}}{(n!)^2 (m!)^2} (kd)^{2n+2m} \frac{(B_0 - 2n)(B_0 - 2m)(m+n)!}{2^{n+m-1}(2m+2n+1)!!}.$$

For numerical calculation it is convenient to combine the terms which involve the same power of kd and obtain

$$R_{11} = \frac{4\pi^3 \rho c d^2}{S_o^4} (kd)^2 \sum_{n=0}^{\infty} \frac{(-1)^n n! (kd)^{2n}}{2^n (2n+1)!!} \sum_{m=0}^{n} \frac{(B_o - 2m)(B_o - 2n + 2m)}{[(n-m)!]^2 (m!)^2} = \frac{4\pi^3 \rho c d^2}{S_o^4} b_o(kd). \quad (46)$$

We note that the factor S_o^{-4} in the expression for R_{11} is just that which is required to make the power proportional to $U_1^2 S_o^{-4}$ and, therefore, finite in the limit. For small kd we see that $b_o(kd) \to (\sigma + 1/2)^2 (kd)^2$ and R_{11} is proportional to $(kd)^2$. For higher values of kd we have evaluated Eq. (46) with the results shown in Table 5.

Table 5

Self Radiation Resistance for a Thin Torus ($\sigma = 0.3$)

kd	$b_o(kd) = R_{11} / \frac{4\pi^3 \rho c d^2}{S_o^4}$	$R_{11}/\rho c A$ for $S_o = 18$
1/2	.151	$.81 \times 10^{-4}$
1	.491	2.65×10^{-4}
$\sqrt{2}$	.891	4.81×10^{-4}
$\sqrt{2.4}$	1.08	5.82×10^{-4}
$\sqrt{3}$	1.44	7.75×10^{-4}
2	2.3	12×10^{-4}

The value $kd = \sqrt{2.4}$ is that for which the quantity $B_o = 0$, and for which there is a perfect null along the axis in the far field pattern, for $\sigma = 0.3$.

Since the surface area of a thin torus is $A = 4\pi^2 d^2 / S_o$ we can write

$$\frac{R_{11}}{\rho c A} = \frac{\pi b_o(kd)}{S_o^3} \quad (47)$$

where $b_0(kd)$ is defined in Eq. (46). Eq. (47) can be used to estimate actual values of the radiation resistance for large, but finite, values of S_0. For example, the "thinnest" ring transducers we are aware of correspond to $S_0 \approx 18$, and for $S_0 = 18$ we give $R_{11}/\rho c A$ in Table 5.

The calculated radiation resistance can be used with the far field pattern expression to obtain the directivity ratio (DR) defined as the ratio of the maximum intensity (in the plane of the ring) to the average intensity. Thus we have

$$DR = \frac{I(\theta = 90°)}{I_{avg}} = \frac{|p(90°)|^2/2\rho c}{\bar{P}/4\pi r^2} = \frac{|p(90°)|^2\, 4\pi r^2}{R_{11} U_1^2 \rho c},$$

and from Eqs. (38) and (47)

$$DR = \frac{(kd)^2}{b_0(kd)} \left[\left\{ 6 + \frac{1}{2} - \frac{1}{3}(kd)^2 \right\} J_0(kd) + kd\, J_1(kd) \right]^2 \qquad (48)$$

In Table 6 the directivity index (DI = 10 log DR) calculated from Eq. (48) is compared with measured values given by McMahon.[12] The values of $b_0(kd)$ in Table 5 were used and the frequencies correspond to $d = 1.72$ cm. The calculated values in Table 6 agree well in magnitude with the measured values, but the frequency dependence of the two differ. However, the frequency range covered in this comparison is not great enough to determine whether this difference has any significance.

Table 6

Directivity Index for a Thin Torus

kd	frequency (kc)	Calculated, Eq. (48), $\sigma = .3$	Measured McMahon's Fig. 7
$\sqrt{2}$	19.7	2.03	2.4
$\sqrt{2.4}$	21.6	2.30	2.4
$\sqrt{3}$	24.1	2.50	2.3
2	27.8	2.65	2.2

The Sound Field on the Axis of the Torus

In addition to the far field there is one other special case in which the general result for the sound field in Eq. (37) simplifies considerably. This is on the z-axis (the axis of the torus) where $S = 1$. From Eqs. (11) and (12) we see that for $S = 1$ and $\eta \neq 0$

$$z(t) = 0,$$

$$X(t) = kd\left[\frac{2}{1-\cos\eta}\right]^{1/2} = k\left[d^2 + z^2\right]^{1/2}$$

With these special values of $z(t)$ and $X(t)$ the integral representation in Eq. (10) immediately reduces to

$$V_{2\ell}(z) = (-1)^{\ell}\frac{2^{2\ell}(\ell!)^2}{(2\ell)!}P_{2\ell}(0)\,h_{2\ell}^{(1)}\left(k\sqrt{d^2+z^2}\right). \qquad (49)$$

For $\ell = 0$ and $\ell = 1$ we have

$$V_0(z) = h_0^{(1)}\left(k\sqrt{d^2+z^2}\right),$$

$$V_2(z) = h_2^{(1)}\left(k\sqrt{d^2+z^2}\right),$$

and Eq. (37) becomes

$$p(z,t) = -\pi\rho c U_1 \left(\frac{kd}{s_o}\right)^2 e^{-i\omega t}\left[(\sigma+\tfrac{1}{2})\, h_o^{(1)}(k\sqrt{d^2+z^2}) + \tfrac{1}{3}(kd)^2\, h_2^{(1)}(k\sqrt{d^2+z^2})\right]. \quad (50)$$

From Eq. (50) we have calculated the pressure amplitude along the z -axis with the results shown in Fig. 16. For $z >> d$ and $kz >> 1$ Eq. (50) reduces to the far field expression in Eq. (38) for $\alpha = 0$. In Fig 16 we have also plotted the far field expression, and we see that it gives the correct result for z greater than about $5d$. Figure 16 shows that the pressure amplitude along the z-axis oscillates before settling down to a steady decrease. This oscillation results from the combination of the two wave functions in Eq. (50). If we had used a velocity distribution which led to only one wave function there would be no oscillation. It would be of interest to compare such calculated results with measurements made along the axis of ring transducers. Such a comparison would help to evaluate the validity of the velocity distribution in Eq. (32) and also help to determine how close to the transducer the far field expression in Eq. (38) remained useful.

Superposition of Thin Torus Fields

Co-axial Arrays of Thin Tori

We now calculate the far field of an array of thin tori which are stacked co-axially as shown in Fig. 17. We can also compare this calculation with measurements published by McMahon.[12] The calculation consists of transforming the result in Eq. (38) for a thin torus with its

Fig. 16 Pressure Amplitude on the Axis of a Thin Torus

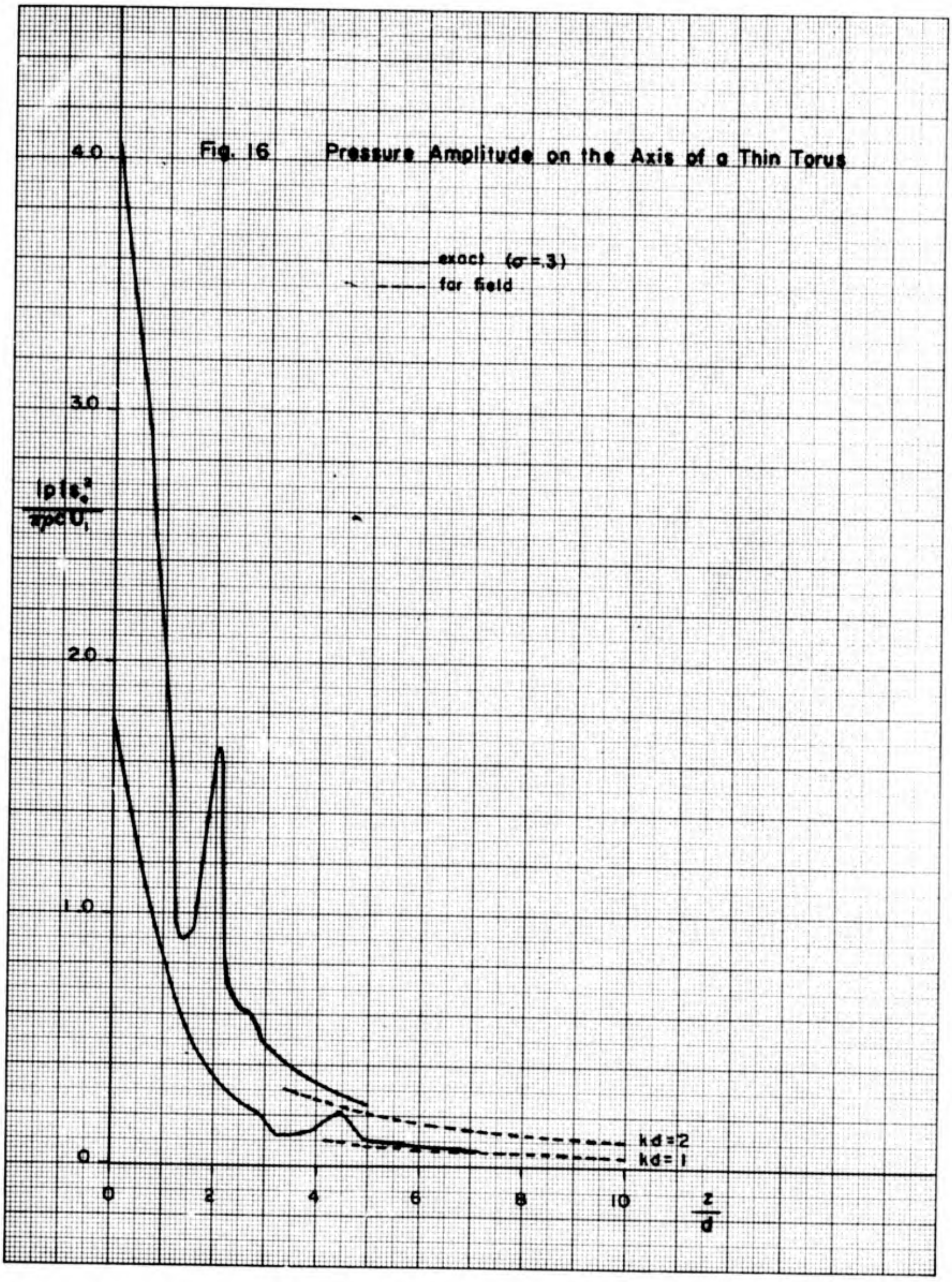

center at the origin to the case where the center is displaced a distance z' along the z-axis. Then the sound pressures for a number of tori at different locations along the z-axis are added to get the resultant field. This simple approach, which neglects scattering between tori, should be a good approximation for our infinitesimally thin tori as long as they are not too close together. However, for a stacked array of ring transducers scattering would be quite important, and we cannot expect detailed agreement between this calculation and measurements.

For a thin torus with its center displaced a distance z' along the z-axis the far field is given by Eq. (38) with r' and θ' in place of r and θ (see Fig. 17). The resulting expression can then be written in terms of r and θ by use of

$$r' = r - z' \cos\theta$$
$$\theta' = \theta$$

which hold in the far field. Carrying out these steps and using the usual far field approximations we obtain

$$p'(r,\theta,z) = i\pi\rho c U_1 \left(\frac{kd}{s_0}\right)^2 \frac{e^{-i(\omega t - kr)}}{kr} e^{-ikz'\cos\theta}\left[(\sigma+\tfrac{1}{2})R_0(\cos\theta) - \tfrac{1}{3}(kd)^2 R_2(\cos\theta)\right] \quad (51)$$

We next add the pressures for N thin tori of the same radius and same velocity with their centers at $z' = 0, h, 2h, \ldots, (N-1)h$ and get

$$p(r,\theta,t) = i\pi\rho c U_1 \left(\frac{kd}{s_0}\right)^2 \frac{e^{-i(\omega t - kr)}}{kr}\left[(\sigma+\tfrac{1}{2})R_0(\cos\theta) - \tfrac{1}{3}(kd)^2 R_2(\cos\theta)\right]\sum_{n=0}^{N-1} e^{-inkh\cos\theta} \quad (52)$$

This result is an example of the product theorem which holds here because all the individual sources have the same pattern and the same orientation. The sum in Eq. (52) is the pattern of N point sources in a line. The

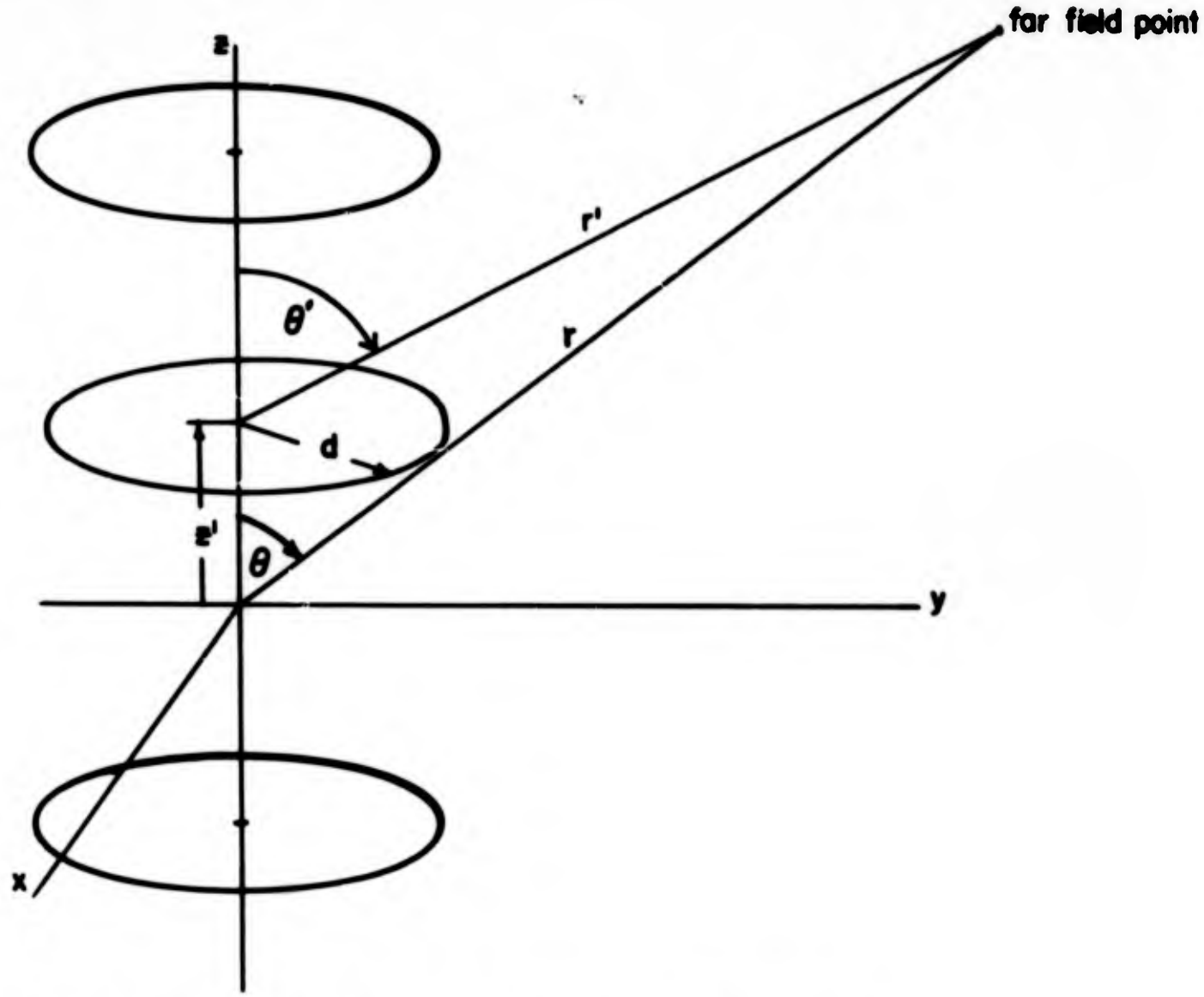

Fig. 17 Coordinates and notation for a stack of thin rings

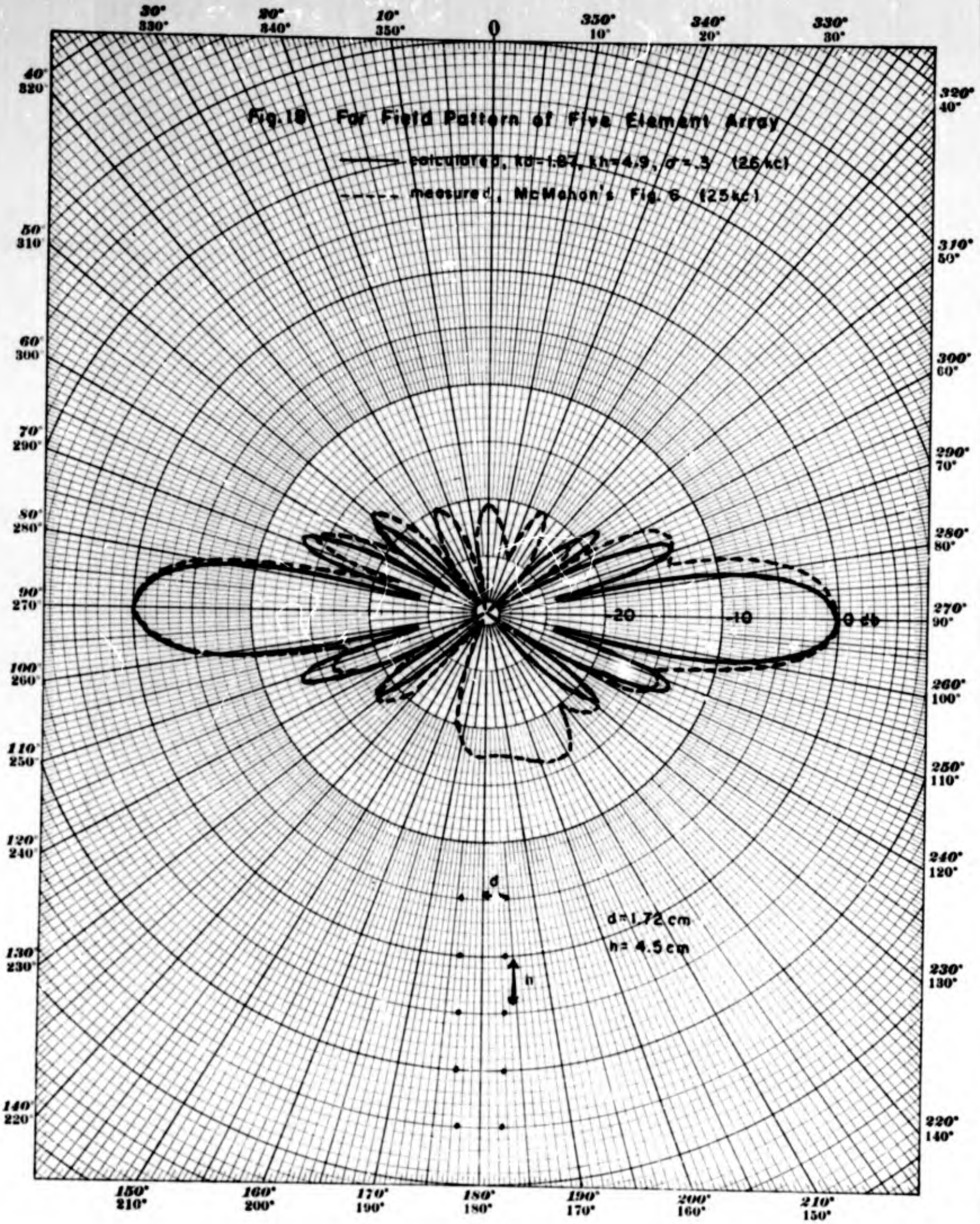
Fig. 18 Far Field Pattern of Five Element Array
calculated, ka=1.87, kh=4.9, σ=.3 (26 kc)
measured, McMahon's Fig. 6 (25 kc)
d=1.72 cm
h= 4.5 cm
d
h
-20
-10
0 db

pressure amplitude obtained from Eq. (52) is

$$|p(r,\theta)| = \frac{\pi \rho c U_1}{kr}\left(\frac{kd}{s_0}\right)^2\left[(\sigma+\tfrac{1}{2})R_0(\cos\theta) - \tfrac{1}{3}(kd)^2 R_2(\cos\theta)\right]\frac{\sin\left(\frac{Nkh}{2}\cos\theta\right)}{\sin\left(\frac{kh}{2}\cos\theta\right)} \quad . \qquad (53)$$

We have calculated the far field pattern from Eq. (53) for an array of five thin tori with $kd = 1.87$, $kh = 4.9$ and $\sigma = 0.3$. This corresponds to McMahon's five element array (for which $h = 4.5$ cm) at 26 kc . In Fig. 18 we compare the calculated pattern at 26 kc with the measured pattern at 25 kc taken from McMahon's Fig. 6. The agreement is quite satisfactory except for directions near the axis of the array (for clarity in the figure we have omitted in the calculated pattern some axial minor lobe structure which is more than 25 db down). A more detailed comparison of calculations with these measurements is pointless, because the measured minor lobe structure near the axial direction is strongly affected by scattering and other factors which have destroyed the symmetry. The portion of these two patterns which are in substantial agreement depends mainly on kh ; therefore, the single element comparison in Fig. 14a provides the more stringent test of the kd dependent part of the pattern.

Mutual Radiation Resistance Between Thin Tori

Next we calculate the mutual radiation resistance between thin co-axial tori by use of the far field approximation for an array of tori developed in the last section. Since this approximation neglects scattering the usefulness of the result for arrays of actual ring transducers may be quite limited. We get the mutual radiation resistance by calculating the power radiated by two co-axial tori separated by a distance h . The

result can then be used for any pair of tori in an array of more than two tori.

If the radiation resistances are referred to U_1 the time average power radiated by two tori can be written

$$\bar{P} = \tfrac{1}{2}\left(2R_{11} + 2R_{12}\right) U_1^2 , \tag{54}$$

where R_{11} is the self and R_{12} the mutual radiation resistance for one torus. As before the power can be calculated from Eq. (43), and with Eq. (53) for the pressure with $N = 2$ we obtain

$$\bar{P} = \frac{2\pi^3 \rho c\, U_1^2}{k^2}\left(\frac{kd}{s_0}\right)^4 \int_0^{\pi} \left[\left(\sigma+\tfrac{1}{2}\right) R_0(\cos\theta) - \tfrac{1}{3}(kd)^2 R_2(\cos\theta)\right]^2 \left[1+\cos(kh\cos\theta)\right] \sin\theta\, d\theta . \tag{55}$$

Comparing the two equations for $\bar{P}$ and using Eq. (44) for R_{11} we find

$$R_{12} = \frac{2\pi^3 \rho c}{k^2}\left(\frac{kd}{s_0}\right)^4 \int_0^{\pi} \left[\left(\sigma+\tfrac{1}{2}\right) R_0(\cos\theta) - \tfrac{1}{3}(kd)^2 R_2(\cos\theta)\right]^2 \cos(kh\cos\theta)\sin\theta\, d\theta . \tag{56}$$

It can be seen that $R_{12} \to R_{11}$ as $kh \to 0$ and $R_{12} \to 0$ as $kh \to \infty$ which is the expected behaviour for the mutual radiation resistance. Furthermore, for small kd the quantity in the square bracket approaches $\left(\sigma + \frac{1}{2}\right)$ and the integral can be evaluated with the result

$$R_{12} \to \frac{4\pi^3 \rho c\, d^2}{s_0^4}(kd)^2\left(\sigma+\tfrac{1}{2}\right)^2 \frac{\sin kh}{kh} , \quad kd \to 0 . \tag{57}$$

This expression has the same dependence on separation h as exists for any small pulsating sources. For small kd the second order toroidal wave function becomes negligible leaving only the zero order function which arises from the pulsating part of the velocity distribution.

The integral in Eq. (56) for R_{12} can be evaluated by expanding the integrand in series as we did for evaluating R_{11} . We obtain

$$R_{12} = \frac{4\pi^3 \rho c}{k^2}\left(\frac{kd}{s_0}\right)^4 \sum_{l=0}^{\infty}\sum_{n=0}^{\infty}\sum_{m=0}^{\infty} \frac{(-1)^{n+m+l}(B_0-2n\times B_0-2m)}{(n!)^2(m!)^2(2l)!\,2^{m+n}}(kd)^{2m+2n}(kh)^{2l}\frac{(2l-1)!!(m+n)!}{(2m+2n+2l+1)!!}.$$

It is convenient to rewrite Eq. (57) as

$$R_{12} = \frac{4\pi^3 \rho c\, d^2}{s_0^4}\sum_{l=0}^{\infty}\frac{(-1)^l(2l-1)!!}{(2l)!}\,b_l\,(kh)^{2l}, \tag{58}$$

where

$$b_l = (kd)^2\sum_{n=0}^{\infty}\sum_{m=0}^{\infty}\frac{(-1)^{n+m}(B_0-2n\times B_0-2m)(m+n)!}{(n!)^2(m!)^2\,2^{m+n}(2m+2n+2l+1)!!}(kd)^{2m+2n}$$

By the same manipulations that led to Eq. (46) we find

$$b_l = (kd)^2\sum_{n=0}^{\infty}\frac{(-1)^n n!\,(kd)^{2n}}{2^n(2n+2l+1)!!}\sum_{m=0}^{n}\frac{(B_0-2m)(B_0-2n+2m)}{[(n-m)!]^2(m!)^2}. \tag{59}$$

The convenient ratio R_{12}/R_{11} can be written

$$R_{12}/R_{11} = 1 + \frac{1}{b_0}\sum_{l=1}^{\infty}\frac{(-1)^l(2l-1)!!}{(2l)!}\,b_l\,(kh)^{2l}, \tag{60}$$

and has been evaluated as a function of kh for $kd = \sqrt{2.4}$. The results are given in Table 7 for values of kh which go high enough to show the location of the first zero of R_{12}. We see that, for $kd = \sqrt{2.4}$, R_{12} is first equal to zero at kh of about 5.3 ($h \approx .84$ wavelengths), while, for small kd, Eq. (57) shows that the first zero occurs at $kh = \pi$ ($h = .5$ wavelengths).

As an example of the use of the mutual radiation resistance we now calculate the directivity ratio for an array of two tori. Using Eq. (54) and following the procedure used in the earlier calculation of

Table 7

Mutual Radiation Resistance for Thin Co-axial Tori

$kd = \sqrt{2.4}$ $\qquad \sigma = .3$

kh	R_{12}/R_{11}
0	1
.5	.980
1.0	.923
1.5	.832
2.0	.717
2.5	.585
3.0	.451
4.0	.203
5.0	.032
5.48	-.016

directivity ratio we now have

$$DR = \frac{|p(90°)|^2 \, 4\pi r^2}{(2R_{11} + 2R_{12}) U_1^2 \rho c} .$$

With Eq. (53) for the pressure with $N = 2$ we get

$$DR = \frac{2(kd)^2 \left[\left\{ \sigma + \frac{1}{2} - \frac{1}{3}(kd)^2 \right\} J_0(kd) + kd \, J_1(kd) \right]^2}{(R_{11} + R_{12}) \Big/ \left(\frac{4\pi^3 \rho c \, d^2}{S_0^2} \right)} , \qquad (61)$$

which shows that except for the influence of the mutual radiation resistance DR for two sources is twice DR for one source. $kd = \sqrt{2.4}$ corresponds to a frequency of 21.6 kc for McMahon's transducers with d = 1.72 cm. At this frequency with h = 4.5 cm we have kh = 4.1, $R_{12} = .18 R_{11}$ and DR equals (2/1.18) times the DR for one torus. Using the value in Table 6 we then find a directivity index of 4.6 db for a two element array. McMahon's measured value is the same to the accuracy with which the curves in his Fig. 7 can be read.

Similar calculations for arrays of more than two elements would require calculation of R_{12} for larger ka. However, if we neglect all but nearest neighbor interactions the total radiation resistance for N equally spaced elements is $NR_{11} + 2(N-1)R_{12}(ka)$. We then have for $kd = \sqrt{2.4}$ and $ka = 4.1$

$$(DR)_N = \frac{N^2}{N + 2(N-1)(.18)} (DR)_1 ,$$

where $(DR)_N$ is the directivity ratio for an N element array. This formula gives values of $(DI)_N$ which are a few tenths of a db greater than McMahon's measured values for 3, 4, 5, and 6 element arrays at 21.6 ka. The overestimate is caused by our neglect of some of the mutual radiation resistances.

Conclusion

The thin torus with an appropriate velocity distribution appears to be a useful theoretical model for predicting far field acoustic radiation from free flooding ring transducers. Reasonable agreement was found between calculations and measurements of the far field pattern and related information such as radiation resistance and directivity index for single transducers and co-axial arrays. The thin torus model has limited usefulness, however; it does not, for example, yield useful results on the radiation mass loading and its important effect on the resonant frequency of ring transducers. To improve the model the present work is being extended in two ways: First, we are doing calculations

for the general torus problem in which the cross section is not vanishingly small. Second, we are beginning calculations for the case of a toroid of rectangular cross section, a model which is very similar geometrically to ring transducers.

Acknowledgement

The writers are grateful for the assistance of Dorothy A. Moran, Nan E. Gordon, Ann R. Parke, and Benjamin T. Howard.

Appendix - Geometrical Relationships

The geometrical relationships which have been used in the text can be derived from the relations between Cartesian and toroidal coordinates;

$$x = \frac{d(s^2-1)^{1/2}\cos\varphi}{s-\cos\eta},$$

$$y = \frac{d(s^2-1)^{1/2}\sin\varphi}{s-\cos\eta},$$

$$z = \frac{d\sin\eta}{s-\cos\eta}.$$

By eliminating φ and η we find that s = constant represents the surface of a torus with (see Fig. 1b)

$$R_1 = d/(s^2-1)^{1/2},$$

$$R_2 = ds/(s^2-1)^{1/2}.$$

It follows that

$$s = R_2/R_1,$$

$$d^2 = R_2^2 - R_1^2.$$

The area and volume of a torus are given by

$$A = (2\pi R_1)(2\pi R_2) = 4\pi^2 s d^2/(s^2-1),$$

$$V = (\pi R_1^2)(2\pi R_2) = 2\pi^2 s d^2/(s^2-1)^{3/2},$$

which are intuitively reasonable and can be proved by integration.

List of References

1) P. Moon and D. E. Spencer, Field Theory for Engineers, Van Nostrand Co., New York, 1961, p. 368.

2) V. H. Weston, Quarterly of Applied Math. 15 420 (1957).

3) V. H. Weston, Quarterly of Applied Math. 16 237 (1958).

4) V. H. Weston, "Solutions of the Toroidal Wave Equation and Their Applications," Doctoral Thesis, Department of Applied Mathematics, University of Toronto, Sept. 1956.

5) PML Staff, "Acoustic Radiation from a Torus," PML Tech. Memo No. 1, Contract N140(70024)75686B, April 1964.

6) M. C. Junger, "A Variational Solution of Solid and Free-Flooding Cylindrical Sound Radiators of Finite Length," CAA Technical Report U-177-48, Contract Nonr-2739(00), 1 March 1964.

7) N. T. Chin, "Self Radiation Impedance of a Finite Free-Flooding Cylindrical Radiator with Junger's End Correction," USNUSL Tech. Memo No. 960-75-64, 25 Aug. 1964.

8) I. M. Ryshik, I. S. Gradstein, Tables of Series, Products, and Integrals, Deutscher Verlag der Wissenschaften, Berlin, 1957, p. 371.

9) P. M. Morse, H. Feshbach, Methods of Theoretical Physics, McGraw Hill Book Co., New York, 1953, p. 1329.

10) J. W. Horton, Fundamentals of Sonar, United States Naval Institute, Annapolis, Md., 1957, p. 176.

11) W. Williams, N. G. Parke, D. A. Moran, and C. H. Sherman (to be published, JASA, December 1964).

12) G. W. McMahon, JASA 36 528 (1964).

BLANK PAGE